INFORMATION TO USERS

This manuscript has been reproduced from the microfilm master. UMI films the text directly from the original or copy submitted. Thus, some thesis and dissertation copies are in typewriter face, while others may be from any type of computer printer.

The quality of this reproduction is dependent upon the quality of the copy submitted. Broken or indistinct print, colored or poor quality illustrations and photographs, print bleedthrough, substandard margins, and improper alignment can adversely affect reproduction.

In the unlikely event that the author did not send UMI a complete manuscript and there are missing pages, these will be noted. Also, if unauthorized copyright material had to be removed, a note will indicate the deletion.

Oversize materials (e.g., maps, drawings, charts) are reproduced by sectioning the original, beginning at the upper left-hand corner and continuing from left to right in equal sections with small overlaps. Each original is also photographed in one exposure and is included in reduced form at the back of the book.

Photographs included in the original manuscript have been reproduced xerographically in this copy. Higher quality 6" x 9" black and white photographic prints are available for any photographs or illustrations appearing in this copy for an additional charge. Contact UMI directly to order.

UMI

A Bell & Howell Information Company
300 North Zeeb Road, Ann Arbor MI 48106-1346 USA
313/761-4700 800/521-0600

Characterizing growth rates and growth rate dispersion of secondary nuclei as a function of supersaturation

by

Christopher Michael Jones

A dissertation submitted to the graduate faculty

in partial fulfillment of the requirements for the degree of

DOCTOR OF PHILOSOPHY

Major: Chemical Engineering

Major Professor: Maurice A. Larson

Iowa State University

Ames, Iowa

1999

UMI Number: 9924727

UMI Microform 9924727
Copyright 1999, by UMI Company. All rights reserved.

This microform edition is protected against unauthorized copying under Title 17, United States Code.

UMI
300 North Zeeb Road
Ann Arbor, MI 48103

Graduate College

Iowa State University

This is to certify that the Doctoral dissertation of

Christopher Michael Jones

has met the dissertation requirements of Iowa State University

Signature was redacted for privacy.

Major Professor

Signature was redacted for privacy.

For the Major Program

Signature was redacted for privacy.

For the Graduate College

TABLE OF CONTENTS

LIST OF FIGURES

LIST OF TABLES

CHAPTER 1. GENERAL INTRODUCTION

Introduction

Crystallization processes are used widely in industry both to purify and separate solid product. They are also useful for generating a specific crystal size distribution. Crystallization from solution, from the melt, and from a vapor are some of the more common techniques used for crystallization, but the most common of these techniques is crystallization from solution.

Driving Force for Crystal Growth from Solution

The dimensionless driving force for crystallization, σ_a, is defined as the difference in the chemical potential between the substance in the supersaturated solution, μ, and in the crystal, μ_{eq} divided by the absolute temperature and the Boltzmann's constant.[1] This can be expressed as

$$\sigma_a = \frac{\mu - \mu_{eq}}{kT} = \nu \ln \frac{a}{a_{eq}} = \nu \ln \frac{\gamma c}{\gamma_{eq} c_{eq}} \tag{1.1}$$

These equations are seldom used in practice. Instead, three approximations are made. First, it is assumed that the activity coefficients are independent of concentration. This is usually a good assumption if the solutions are dilute or if c and c_{eq} are close together. Second, ν, the number of ions per molecular unit, is set equal to unity, which is only true for non-electrolytes. Thus,

$$\sigma_a \cong \ln \frac{c}{c_{eq}} = \ln(\sigma_c + 1) \tag{1.2}$$

where,

$$\sigma_c = \frac{c - c_{eq}}{c_{eq}} \tag{1.3}$$

Then approximating that $\sigma_c << 1$, σ_a reduces to

$$\sigma_a \cong \sigma_c \tag{1.4}$$

Supersaturation, σ_c ,is used to characterize the driving force for most crystallization models as it provides a means of calculation from measurable solution properties.

Supersaturation of solute in solution is generally caused by either cooling of the solution, evaporation of the solvent, or by salting out. Salting out involves adding a more soluble solute to the solution causing the less soluble solute to become supersaturated. For example, by cooling a saturated, solution it becomes supersaturated. In order to reach equilibrium and minimize the free energy of the system, crystallization of the supersaturated solute occurs.

The Complex Nature of Crystallization

Crystallization is a multi-component, multi-phase process that involves simultaneous heat and mass transport to the crystal surface. The relationships between nucleation, growth, and various process characteristics are complex and interactive. For example, growth rates are dependent on many factors such as: birth rates, nucleation mechanism, supersaturation, mixing rates, flow patterns, solvent, contaminant concentration, temperature, residence time distributions, nucleation rates, and growth rate dispersion (GRD). Growth rate dispersion is the phenomenon where crystals nucleated by the same mechanism, and grown under the same conditions exhibit different growth rates.

Nucleation plays another key role in determining crystallization behavior. Nucleation is dependent upon supersaturation, slurry density, crystal size distribution, mixing rates, impeller material, solvent, contaminant concentration, flow patterns, temperature, growth rates, and growth rate dispersion.

Using the theoretical population balance of Randolph and Larson[2], assuming steady state mixed suspension mixed product removal continuous crystallization with no growth rate dispersion, the relationships between nucleation and growth rates gains some clarity.

For steady state mixed-suspension mixed-product removal (MSMPR) operation, Randolph and Larson determined the population density to be:

$$n = n^o \exp(\frac{-L}{G\tau}) \tag{1.5}$$

Plotting the log of n versus size yielded a linear fit where the intercept at L=0 is n^o and the slope of the line is $-1/G\tau$. Using the assumption of constant growth rate for all crystals and the assumption that crystals are born at zero size, one can formulate a relation for the birth rate of nuclei:

$$B^o = Gn^o \tag{1.6}$$

The population of crystals at size L=0, n^o, moves along the size coordinate with a constant velocity of G. Multiplying the two terms yields the rate at which new crystals are formed, B^o. Similarly the number of crystals per time that grow from size L to size L+dL is Gn(L).

Significance of GRD

Growth rate dispersion causes deviations from the theoretical population balance. In MSMPR crystallizers operating at steady state, growth rate dispersion often causes strong

upward curvature of the semi-logarithmic plot of the population density versus size at small sizes. GRD results in higher than predicted nucleation rates and alters the predicted product size distribution. Unless it is accounted for, GRD also causes large errors in design and scale up of crystallization processes.

The purpose of this work is to enhance the modeling of crystallizers through the examination and characterization of the growth rate dispersion phenomenon. Relatively little information has been gathered which characterizes GRD as a function of system conditions. As a result, crystallization processes remain difficult to predict and to control. Understanding what causes some crystals to grow and others not to grow will make for better modeling and, hopefully, more efficient ways of carrying out the crystallization process.

Literature Review

Growth Rate Dispersion (GRD)

Growth rate dispersion is the phenomenon where crystals nucleated by the same mechanism and exposed to constant conditions of supersaturation, temperature, and hydrodynamics grow at different rates. Growth rate dispersion, which is present to varying degrees in most systems, causes deviations from what is predicted by theory. The most visible effect of growth rate dispersion is strong upward curvature of the plot of the log of population density versus size at small sizes--nuclei.

Confirming the Existence of GRD

The upward curvature in the semi-log plot of population density vs. size for crystals in the small size ranges <100 mm was a large concern. Some systems, like potassium sulfate-water[3], exhibit curvature throughout the whole CSD. Size dependent growth (SDG),

commonly held to explain this curvature, attributes the strong upward curvature at small sizes to the theory that small crystals grow slowly while large crystals grow rapidly. This was determined by reasoning that a large slope on the semi-log plot of crystal size and population density indicates the growth rate is slow and a smaller slope indicates a large growth rate. While SDG provided a means of modeling this curvature, SDG has been shown to be a manifestation or misinterpretation of the GRD phenomenon; [4]Table 1.1 provides a number of sources that confirm this.

Table 1.1 Papers confirming growth rate dispersion[5]

Authors	System
Berglund and Larson (1984)[6],	citric acid monohydrate-water
Ramanaryanan (1982)[7]	ammonium dihydrogen phosphate- water
Berglund, Kaufmann, and Larson (1983)[8]	potassium nitrate-water
Shanks and Berglund (1985)[9]	sucrose-water
Mathis-Lilley and Berglund (1985)[10]	potash alum-water
Garside and Ristic (1983)[11]	ammonium dihydrogen phosphate-water
Ramanarayanan, Berglund, and Larson (1985)[12]	citric acid monohydrate-water
Ramanarayanan, Berglund, and Larson (1985)[13]	ammonium dihydrogen phosphate-water
Girolami and Rousseau (1985)[14]	potash alum-water
Elankovan and Berglund (1987)[15]	dextrose-water
Teodossiev (1987)[16]	ammonium-alum-water
Liang, Hartel, and Berglund (1987)[17]	sucrose-water

The growth rate distribution of nuclei provides information on the number of nuclei that will reach the upper sizes of the CSD. If one is able to better control and understand the physical processes involved with nuclei GRD, then one should also be able to control and predict the crystallization process behavior with more precision. In addition, characterizing growth rate dispersion provides insight into crystal growth and its relationships with other process characteristics.

Modeling Growth Rate Dispersion

Random Fluctuation Model. Growth rate dispersion was first discussed with respect to how it affects the crystallization process by White and Wright[18]. They were studying the batch crystallization of sucrose when they noticed that as time progressed the variance of the crystal size distribution (CSD) increased. They termed what they saw as size dispersion. They observed a relatively linear relationship between the variance of the CSD and time. In a batch crystallizer one might expect that as supersaturation decreases the growth rate of crystals in the crystallizer would decrease but the CSD would not widen unless the growth rates of crystals in the crystallizer are not constant.

Randolph and White[19] proposed the first set of equations modeling growth rate dispersion (GRD) using what they termed the random fluctuation (RF) model. Their model considered that a crystal's growth rate would fluctuate randomly over time. These random fluctuations are said to result from the fundamental mechanism of crystal growth due to surface imperfections and lattice dislocations. Thus as crystals grow, surface dislocation density, and hence, intrinsic growth rate can change as crystals form and overgrow imperfections. The process is repeated continually and randomly. Similar and more severe fluctuations in growth rate occur with poor agitation where crystals travel through different zones of supersaturation.

Randolph and White hypothesized the following as causes of size dispersion in their batch crystallizer:

- Distribution of residence times in a continuous discharge process.
- Spatial or temporal distribution of nucleation in plug or batch process.

- Size dependent growth (SDG).
- Size dispersion due to random fluctuations in growth rate.
- Size dispersion due to Taylor diffusion in plug flow configurations.

A molecular diffusive flux is produced when a concentration gradient is imposed on a randomly fluctuating molecular velocity field taken relative to a gross average velocity of the flow field. Analogously, a population diffusion can occur when members of a crystal distribution grow at randomly different velocities relative to a mean growth rate. This gave rise to the growth diffusivity, D_G. Size spreading might also occur as a result of axial diffusion in a plug flow crystallizer, giving rise to an axial diffusivity term, D_A. The growth and axial diffusivities are then incorporated into the population balance yielding the micro and macro balances respectively:

$$\frac{\partial n}{\partial t} + v_z \frac{\partial n}{\partial z} + \frac{\partial (Gn)}{\partial L} = B - D + D_A \frac{\partial^2 n}{\partial z^2} + D_G \frac{\partial^2 n}{\partial L^2} \tag{1.7}$$

$$\frac{\partial n}{\partial t} + \frac{\partial (Gn)}{\partial L} + n \frac{\partial (\log V)}{\partial t} = \sum_i \frac{\overline{Q}_i n_i}{V} + B - D + D_G \frac{\partial^2 n}{\partial L^2} \tag{1.8}$$

Using the population balances to find the moments of the population balance, data from a crystallizer could then be used to determine the value of D_G. For a batch crystallizer D_G could be determined by plotting either s^2, the variance of the CSD, against either time or average size, L. The following relationships use the linear relation observed by White and Wright to determine the growth diffusivity.

$$\frac{\Delta s^2}{\Delta t} = 2 D_G \tag{1.9}$$

$$\frac{\Delta s^2}{\Delta L} = \frac{2D_G}{G} \tag{1.10}$$

Alternatively, Tulke and Offermann[20] used the results of Human *et al.* and Ristic *et al.* to show how the parameter D_G can be calculated from single crystal experiments of potash alum.

If the method of growth rate dispersion is truly due to random fluctuations then one should see a linear relationship as shown in the previous two equations. If this exists then the growth diffusivity is readily calculable and can be added to the population balance equation. While the RF model may provide adequate fits to data, experimentation has shown that the random fluctuations of crystals' growth rates are not the primary source of size dispersion in a crystallizer.

Constant Crystal Growth Model. The second model used to model the growth rates is the constant crystal growth (CCG) model. The CCG model makes the following assumptions:

- Contact nuclei are produced in a variety of sizes.
- Different crystals have different linear growth rates.
- Growth rate is constant not size dependent.
- There is inconclusive evidence of a correlation between growth rate and initial size.

Instead of assuming that all crystals undergo random fluctuations in their growth rate, one assumes instead that each individual crystal has an inherent and constant growth rate. Ramanarayanan[21] observed that individual crystals growing under the same conditions nucleated from the same parent crystal, though having different growth rates from one

another, had constant growth rates. CCG has been supported for different systems and varying nucleation mechanisms.

Modeling Continuous and Batch Processes Using GRD. Berglund and Larson[22] presented a mathematical model for predicting the CSD from a continuous crystallizer when strong GRD effects are present. Assuming that the growth rates of crystals in a crystallizer are distributed according to a gamma distribution, they demonstrated that GRD can be misinterpreted as SDG. Observations of nineteen KNO_3 nuclei plotting characteristic size vs. time demonstrated that all nuclei had linear growth rates and non-zero intercepts. They also observed that some nuclei did not grow, and they hypothesized that this was a structural effect.

Garside and Ristic[23] used both log-normal and gamma distributions to model the growth rate distributions of ADP crystals. They also observed, while looking at the growth rates of the 111, 100, and 110 faces over time, that there are no random changes in the growth rates. They observed CCG. In addition, Garside and Ristic saw no difference in the magnitude of dispersion for different faces. Zikic, Ristic, and Sherwood[24] later expanded the modeling of the growth rate distribution to include three parameter distributions accounting for the possibility of some crystals having negative growth rate or dissolving back into solution.

A new form of the population density function was developed using a bivariate distribution for crystals in the crystallizer by Janse and de Jong.[25]

$$n(L) = N_T \int_0^{\infty} f(G, L) dG = N_T f(L) \tag{1.11}$$

and,

$$f\left(\frac{L}{G}\right)=\frac{f(G,L)}{f(G)} \tag{1.12}$$

The function f(G,L) is the joint probability density function of a crystal in the crystallizer having a growth rate G and size L. The function f(L/G) is the conditional probability density function of size at a given growth rate. GRD could be used to demonstrate marked curvature of a semi-logarithmic population density vs. size plot for a mixed-suspension, mixed-product removal (MSMPR) crystallizer in the absence of SDG. Berglund and Larson[26] suggested that the apparent SDG is a result of the washing out of slow growing crystals. The growth rate distribution was shown to have a large and statistically significant effect on the product CSD, while the initial size distribution was shown to have a statistically significant effect despite a large scatter in the data. However, requiring the growth rate be dependent on the initial size does not significantly alter the results. This conclusion concurs with the earlier results of Garside studying small potash alum nuclei.

Larson, White, Ramanarayanan, and Berglund[27] describe a technique for determining the mean and variance of a growth rate distribution using the CSD of an MSMPR crystallizer. Conversely, the CSD can be predicted by prior knowledge of the growth rate distribution. The results are presented such that the growth rate distribution to be determined had the form of either a gamma, inverse gamma, or a log-normal distribution. Gupta and Bhatia[28] present an alternative method of finding the growth rate distribution using regularization which yields virtually the same results as other methods.

Work performed by Berglund and Murphy[29] demonstrated that for their citric acid and water system the RF and CCG models fit their data equally well. However, examination of individual crystals' growth rates over time indicates that the CCG model is favored. Zumstein and Rousseau,[30] considering the possibility that random growth fluctuations might damp out the effects of there being a growth rate distribution, combined the RF and CCG models with success to fit systems that exhibit either or both RF and CCG. For an isothermal batch crystallizer with negligible breakage nucleation,

$$\frac{\partial f(L|G)}{\partial t} + G\frac{\partial f(L|G)}{\partial L} = D_G \frac{\partial^2 f(L|G)}{\partial L^2} \tag{1.13}$$

and for an MSMPR crystallizer with negligible breakage nucleation,

$$G\frac{df(L|G)}{dL} - D_G \frac{d^2 f(L|G)}{dL^2} = -\frac{f(L|G)}{\tau} \tag{1.14}$$

They used the combined RF and CCG model with success to model a potash alum and water system for both batch and MSMPR crystallizers.

Bohlin and Rasmuson[31] confirmed that the influence of GRD on the CSD of batch cooling crystallizers is significant even at moderate dispersion. At high dispersion, the shape of the growth rate activity distribution may become important. Their model accounts for primary and magma density-dependent secondary nucleation mechanisms and uses the CCG type dispersion model. The study includes three different growth rate activity distributions and the influence of the corresponding coefficient of variation is analyzed for seeded and unseeded processes.

Size Dependent Growth (SDG). Bohlin and Rasmuson also observed, as have other researchers, that a crystal's growth rate is not dependent upon its size, i.e. no size-dependent

growth. Early work in characterizing what was causing GRD and how to control it originated with the idea of size dependent growth (SDG). SDG theory states that a crystal's growth rate was somehow dependent upon its size at any time. The most basic idea of SDG was that small crystals grew slowly and large crystals grew rapidly. However , work confirming the validity of the CCG model of crystal growth demonstrated conclusively that size-dependent growth was not correct.

Girolami and Rousseau[32] and Wang, Mersmann, and Kind[33] demonstrated that earlier observations of SDG in the potash alum-water system are a manifestation of GRD; in addition, they verified the CCG model for attrition particles in both a stagnant and flow through cell. It is interesting to note that despite the fact that SDG is not valid, it was still used industrially in continuous crystallization processes to model processes that exhibited a large degree of curvature over part or all of the CSD. The SDG model provided good correlations to experimental data; however, SDG has outdated its validity.

Characterizing Growth Rate Dispersion and Related Phenomena

In work performed by Garside[34] and by Berglund, Kaufman, and Larson[35], a statistically significant correlation between the growth rate of a crystal and its initial size was presented, but there was a large degree of scatter. Garside studied the growth rates of individual potash alum crystals in the size range of 3-40 μm. He observed not only that some small crystals do not grow at all following their nucleation, but also that each crystal possessed its own intrinsic, constant growth rate.

Garside[36] provides an explanation of why small crystals do not grow despite significant supersaturation. The Gibbs-Thompson effect is not considered applicable because

the crystals' characteristic sizes are all larger than 1μm. However, Garside suggests that the mechanism by which nuclei are formed causes the formation of *hills* and *valleys* on the crystal surface such that the radius of curvature is sufficiently small to see a localized Gibbs-Thompson effect on the crystal surface. In the vicinity of the hills, the curvatures are such that one sees an increase in the solubility. While in the valleys, the curvature is in the opposite direction so the solubility will be lower. Thus, the while the hills tend to dissolve the valleys grow and the surface becomes flat. During this change, the overall size of the crystal as measured would not change. From this perspective, the Gibbs-Thompson effect would be significant on crystals greater in size than 1mm provided the crystal surface is not bounded by flat, low index planes. However, it is difficult to understand why such processes should interfere with the normal growth of the crystal as a whole.[37] An examination of ripening times for nuclei with local radii of 0.1 μm confirms that an hour would be sufficient for the surface to flatten. For smaller radii this time might be only a few seconds. This is significantly lower than the time reported of up to 4 hours for zero growth.

Modeling Crystal Growth

Models to predict the growth rates of crystals in a crystallizer from the physical properties of the system, such as temperature and supersaturation, have existed for many years. Some of the more important models are presented to illustrate the various physical interpretations of the rate controlling step of crystal growth. Complete and thorough coverage of various growth models can be found in Pamplin[38], Mullin[39], Strickland-Constable[40], Ohara and Reid[41], Hartman[42], and Benema[43].

Mononuclear Two-Dimensional Nucleation Model.[44] This model assumes that the rate limiting step is the formation of a critical sized embryo. Once formed on the crystal surface, the subsequent lateral growth on the surface is infinitely rapid. The growth rate normal to any face of total area, A, with step height, h, and nucleation rate of critical sized nuclei per unit area, I, is

$$G = AIh \tag{1.15}$$

If this model is correct then the growth rate ought to be proportional to the area of any face, A. Experimentation has not found any such relation between the two which makes the model appear unsatisfactory.

Polynuclear Two-dimensional Nucleation Model.[45] Removing the assumption of an infinite lateral spreading velocity and replacing it with the assumption of a spreading velocity of zero, growth occurs simply by the accumulation of critical size embyros. The growth rate normal to any face with step size, h, nucleation rate, I, and critical embryo size, ρ_c, is

$$G = \pi \rho_c^{\,2} hI \tag{1.16}$$

There is no area dependency in this model, but both ρ_c and I are functions of S_B, the solution supersaturation.

$$S_B = \frac{c}{c_{eq}} \tag{1.17}$$

As S_B increases, I increases, but ρ_c decreases. Consequently, one should find a maximum in G at some value of S_B. This constraint is not observed experimentally making this model inadequate.

Birth and Spread Models.[46] The birth and spread model is an intermediary between the previous two models. In this model, critical sized embryos form on the crystal surface and grow laterally at some finite rate. The exact rules relating the lateral spreading velocities to system parameters are the main difference between the different birth and spread models. In general, the final equations describing the growth rate of a crystal are complex functions of supersaturation and temperature. G increases both with S_B and T; however, no maximum of G with S_B is predicted. There is no dependence on crystal area.

In general nucleation models are not satisfactory in predicting or correlating crystal growth rates in solution. The nucleation models do not account for GRD, while some of the constraints like unusual dependence on area or supersaturation have already been mentioned. In addition, it was found that at low values of S_B the predicted values of the growth rate are much less than one sees experimentally.

Surface Diffusion and Dislocation Theories. Burton, Cabrera, and Frank[47] (BCF) put forward their dislocation model in 1951. This model assumes that a step in the form of a screw has, as its origin, a screw dislocation, a crystal fault known to exist in many crystals. This screw dislocation is self-perpetuating. No new steps would have to be generated. Solute molecules from the bulk adsorb on the flats between steps, migrate under a surface concentration gradient to the steps, and become incorporated into the lattice. The BCF model analyzes first the growth of a straight step with incorporation of surface adsorbed molecules. The partial differential equations of diffusion are solved allowing for concentration gradients along the surface as well as along the actual step between kinks.

Chernov[48] put forward a simplified version of the BCF model assuming that the distance between two successive kinks is so small that one can consider a step as a line sink. This makes any concentration gradient a function only of the direction normal to the crystal face and normal to the step instead of being functions of three dimensions.

Bennema[49] describes the use of statistical mechanical Ising models and Monte Carlo computer simulation, along with transport models, to model growth rates of crystals. These models also allow for the characterization of a crystal's surface; the results of these simulations have been positive being able to describe the growth spirals observed on many crystal surfaces. The concept of surface roughness is used to characterize a surface and thereby its growth. As crystals in a process most likely have different surface roughness' and varying numbers of screw dislocations associated with them, they will have different growth rates as a result.

Dislocation models have a large degree of ambiguity. The physical constants that make up the model are not easily measurable, but from a physical standpoint this model seems very reasonable. Screw dislocations have been observed experimentally using x-ray surface topography, and they can account for GRD.

Mass Transfer Limited Growth. Assuming that the rate of incorporation of solute at the crystal surface is infinitely rapid, the rate limiting step is the transfer of solute from the bulk to the surface. In such models, the concentration at the surface is always assumed to be at equilibrium, but experimentation has shown that the concentration of solute at the crystal surface is usually supersaturated. One can then describe the rate of growth of the crystal, on a mass basis, by looking at the flow of solute, J, to the surface with an area ,A, using a mass

transfer coefficient k_c. The driving force for mass transfer limited growth is the difference between the concentration of solute at the crystallizer conditions and the equilibrium or saturated concentration, c_{eq}.

$$J = k_c c_{eq} S_B A \tag{1.18}$$

The mass transfer coefficient is often correlated as a function of fluid dynamics and solution properties. The Frossling equation is often used to find k_c by relating the dimensionless Reynolds, Sherwood, and Schmidt numbers. For a spherical crystal, the Frossling Equation is:

$$N_{Sh} = 2 + 0.6 N_{Re}^{1/2} N_{Sc}^{1/3} \tag{1.19}$$

Garside[50] performs a detailed analysis of the role of transport processes on the growth rate of crystal from solution. He used the concept of an effectiveness factor, used often in modeling catalytic reactions, to take into account the importance of heat transport, mass diffusion and integration resistances.

Allowing for GRD. Only the BCF model allows for the possibility of GRD. Garside and Davey[51] state that since this model is structure sensitive, it must allow for variation in growth rate from surface to surface of different crystals. For the BCF model, by varying the number of dislocations and the various groupings of growth spirals, the overall growth rate would be a non-integral multiple of R, the growth rate for a single growth spiral. Within the BCF formalism, this variation in growth rate is introduced via the parameter ε which quantifies the extent to which a group of dislocations enhances the growth rate of a face compared to a single dislocation.

$$G = C\sigma_1\varepsilon\left(\frac{\sigma}{\sigma_1}\right)^2 \tanh\left(\frac{\sigma_1}{\varepsilon\sigma}\right) \qquad (1.20)$$

Thus, one can plot curves of the normalized growth rate ($G/C\sigma_1$) as a function of (σ/σ_1) for different values of ε. For ε values below 5, the kinetic curves are clear and should be experimentally demonstrable. For ε values above 5, the curves become increasingly close together such that for ε values of 7 or 8 they are not distinguishable. Hence, for a given population of crystals, equivalent crystal surfaces will show growth rate dispersion provided the operative values of ε are smaller than 5. This is not unreasonable since the probability of finding a dislocation in a crystal will increase with both the growth time of that crystal and the energy of collisions which it experiences. This probability will thus increase with size with a corresponding increase in ε.

Valcic[52] and Davey *et al.*[53] provide quantitative evidence that growth rate dispersion is due to dislocations. Valcic measured 100 face growth rates of sucrose crystals in the size range 40 to 100 μm and found that the kinetic data fitted a series of BCF curves corresponding to ε values between 1 and 5. Davey *et al.* found similar results for the 100 face of $NH_4H_2PO_4$ crystals.

Harris describes a microscopic theory of crystal growth that is a modified form of the BCF theory[54]. He uses the Fokker-Planck equation to describe the diffusion of molecules along terraces. The fundamental rate determining process in the BCF model depends upon the surface diffusion along the terraces to the stationary steps. Diffusion to the terraces from the bulk and to the kinks in a given step are considered to be fast processes not requiring theoretical elaboration for a clear understanding of the overall growth mechanism. An

essential ingredient in these theories is the use of a macroscopic diffusion equation incorporating Fick's law relating the surface flux and density. The new model then is a reexamination of this surface diffusion process from a microscopic viewpoint.

The Role of Dislocations and Lattice Strain on GRD

Ristic, Sherwood, and Shripathi[55] provide experimental evidence of the role of dislocations and mechanical deformation in GRD of potash alum crystals. They performed their studies using a growth cell with a tensile straining device on which a crystal was mounted. This allowed for the crystal to be examined under stress free conditions and then strained to fracture in a controlled manner. Large crystals of potash alum ~2 cm were used to discern the effects of dislocations and applied mechanical deformation on the growth rates of specific faces.

In addition, small microcrystals, formed by a secondary nucleation mechanism, were tested for their integral strain. The growth rates of these crystals in the 100 direction was then related to the integral strain to determine if the level of strain had a significant effect on their growth rates.

Dislocation characterization and assessment were carried out using X-ray transmission topography while synchrotron Laue techniques were used to determine the integral strain (mosaic spread) of microcrystals formed by secondary nucleation.

Strain induces a radial asterism, M, in the diffraction spots on the Laue patterns. This is related to the mosaic spread by the expression:

$$2\eta = \arctan\left(\frac{M-S}{B_s}\right)\cos^2 2\theta \qquad (1.21)$$

where B_s is the sample to film distance and θ is the Bragg angle of the reflection chosen. S is the undistorted diffraction spot size and is given by:

$$S = D_l + t' \bullet \tan\theta \qquad (1.22)$$

where D_l is the diffraction length and t' is the specimen thickness.

Variations in Growth Rate Caused by Varying Dislocation Density. Ristic *et al.*[56] demonstrated, parallel with the results of Human *et al.*[57], that short term variations in growth rate occur mainly on the 110 and 100 surfaces for large potash alum crystals, while the 111 surfaces have uniform growth rates. The 111 surface growth rate is also constant over long periods of time. However, the growth rate of the 110 face is constant for about two hours before it becomes variable and decreases. Eventually, it levels out to a low average growth rate about which the growth rate fluctuates.

Ristic *et al.*[58] explained this behavior by examining the dislocation structure of a large growing crystal using X-ray topography. A dark line around the seed marks the boundary between the seed and new growth. New growth dislocations propagate from this region developing normal to the growing surface. This boundary is a source of a large number of dislocations and as a consequence it is also a source of high levels of strain. Because the 100 or 110 facets were growing more rapidly than the adjacent 111 facets the area of the fast growing facets will decrease. This results in the growth sector developing a wedge shape thickest at the seed end. Some of the propagating dislocations in the fast growing growth sectors will intersect at this boundary and cross into the adjacent 111 growth sector. Examination of the X-ray topograph confirms that some dislocations appear to end within the image with a curl at the tip which defines the start of their new orientation into a new growth

sector. This loss of dislocations from the 100 and 110 growth sectors accounts for the decrease in their growth rates.

Ristic *et al.*[59] suggest that a screw/mixed dislocation mechanism dominates on the 111 surface while an edge dislocation, two dimensional birth and spread growth mechanism dominate on 100 and 110. The 100 growth sector has edge dislocations formed predominately at inclusions. The 110 growth sectors were often dislocation free, while the 111 growth sector is the most defective containing dislocations of all characters-edge, screw, and mixed.[60]

Dependence of Dislocation Density of 100 Surface of Potash Alum on Supersaturation. Ristic *et al.*[61] demonstrated experimentally that the dislocation density of the 100 surface of seeded potash alum crystals could be controlled by changing the rate at which a seed was re-facetted. The re-facetting rate was controlled by changing the supersaturation of the solution that seeds were introduced into; the higher the supersaturation, the faster the re-facetting occurred and the greater the dislocation density. Crystals grown at equivalent supersaturations, but re-facetted at different supersaturations, exhibited growth rates that were dependent upon the dislocation density at the interface. However, crystals still exhibited growth when no dislocations were present.

Variations in Growth Rate Due to Strain. Variations in the growth rate may also be a result of the development of strain in the crystals either by impurity incorporation or growth sector boundary overlap.[62] Large potash alum crystals were mounted in the cell and growth was initiated. Once the growth rate had become constant with time a mechanical stress was applied to the crystal using the forementioned straining device and the growth rate

diminished to zero. Removal of the strain resulted in a return to normal growth behavior. This behavior was completely reversible. Successive applications, using lower amounts of stress while the crystal was growing, caused reductions in the growth rate, but the growth rate could be restored by either reducing the stress or by increasing the supersaturation. X-ray topography of crystals subjected to these trials demonstrated that no significant structural changes had occurred within the growth boundary that this behavior could be attributed to. Mechanical dislocations that did yield dislocations, which intersect the growing interface, had a noticeable influence on growth.

Using double crystal diffractometry, the development of strain was mapped against the growth sector boundary. This boundary is highly strained; this can be seen by its high contrast in the X-ray topograph. The strain variation oscillates reaching a maximum at each constriction of the growth sector boundaries. The strain developed at these constrictions was approximately that which the experiments using applied mechanical stress showed would cause a significant slowing of growth. Ristic *et al.*[63] provide two potential causes for this effect:

1. Undetectable amounts of impurity could on adsorption at the interface slow the growth and yield a gradual build up of strain in the surface. Growth could stop either as a result of the impurity or of strain. The area of the face would expand until the supersaturation built up high enough that nucleation would occur on the poisoned surface. Rapid growth could include the poisoned layer.
2. The growth sector boundaries were highly strained. As they approach each other during rapid growth a point might be reached where the total strain developed in the material in

the sector causes a growth arrest. Sudden overgrowth as the supersaturation could cover the strain and growth would continue.

Samples of small crystals, formed by secondary nucleation, were grown in solution and tested for their integral strain using Laue diffraction. The growth rates show a well-defined variation with mosaic spread. The crystals with the highest growth rates have the lowest levels of strain, while the crystals with the lowest growth rates have the highest levels of strain. This result was also found for secondary nuclei of sodium chlorate by Ristic, Sherwood, and Wojciechowski.[64] Sodium chlorate exhibited a higher dependence of growth rate on strain than potash alum. Ristic *et al.*[65] associated this with the fact that sodium chlorate is more brittle than potash alum. In addition they deduced that sodium nitrate is ductile and shows no significant variation in included strain.

Using Strain to Model Growth Rates

Van der Heijden and van der Eerden[66] proposed several physical models which relate the mosaic spread found in secondary nuclei to the phenomenon of GRD:

- Point defects.
- Random distribution of dislocations.
- Grain boundaries.
- Volume strain variations in crystals.

Comparison of theoretical models with available experimental data, from Ristic *et al.*,[67] indicate that the most relevant picture is to assume the presence of low-angle grain boundaries in the secondary nuclei that influence the growth rates of these crystals. The length scale associated with these grain boundaries is on the order of 0.5-1.0 μm and can be

qualitatively understood from the length scale involved in abrasion processes. The proposed growth rate expression incorporates integral lattice strain and also the size of the crystal implying size dependency.

When secondary nuclei were produced, due to fluid shear or an attrition mechanism for example, these crystals will not be faceted in general. During growth the non-habit faces will disappear, but stress will be built up at the interface along with a high dislocation density. After some time the new crystal becomes faceted and the growth of new stressed regions will decrease. It seems likely that the growth of new stress regions will decrease. In the case of ductile materials, like sodium nitrate, it is more likely that contact with stirring device or wall of the crystallizer might cause the formation of new dislocations and new regions of strain than it would be for other materials.[68] It appears likely that most stressed areas were formed during the re-facetting process, while after that period the growth is more perfect. Since the time needed for re-facetting is on the order of 10-100 ms for a particle of size ~10 μm [69]this process is completed very rapidly, which is another reason for less perfect growth.

Varying amounts of dislocations were an obvious way of explaining differences and fluctuations of growth rate in secondary nuclei. Secondary nuclei have a large amount of dislocations and, as a result, are highly stressed. The presence of stress means that this stress energy must be added to the internal energy of the crystal. This implies that the free energy and, as a result, the chemical potential of the crystal were increased thereby decreasing the driving force for growth.

One can consider secondary nuclei as imperfect crystals built up from smaller blocks that are all slightly misoriented with respect to one another. Thus, the mosaic structure of a crystal is a three-dimensional network of low-angle grain boundaries. Each grain boundary is an array of dislocations. Due to this mosaic structure, Laue diffraction spots become streaks rather than the usual circular spots one sees in the case of perfect crystals similar to most metals. It is the radial elongation of these streaks or spots which is measured and then related to the mosaic spread, η, which is the effective deviation in orientation of an X-ray having passed the crystal. The mosaic spread is an indirect measure of the average misorientation or misfit angle between the mosaic blocks in the crystal.

Strain and Crystal Perfection: Effects in an MSMPR

Zacher and Mersmann[70] examined integral lattice strain effects on GRD in a continuous suspension potash alum crystallizer. As presented earlier by van der Heijden *et al.*[71], the most relevant physical picture of how lattice strain effects crystal growth is the low angle grain boundary model. Zacher and Mersmann present crystal perfection analogous to the average misfit angle θ_m deduced from Laue diffraction. If η is the mosaic spread of a crystal, L' is the radius of the irradiated region, and l is the average size of the mosaic blocks, which were assumed to be cubic and generally on the order of a micron, then

$$\eta = \left(\frac{L'}{l}\right)^{\frac{1}{2}} \theta_m \tag{1.23}$$

Their results confirmed that the mean misfit angle for crystals of the same size increased with increasing supersaturation. The standard deviation of the mean misfit angle also increased with increasing supersaturation. Thus, at low supersaturations crystals had

higher perfection and lower misfit angles, while at higher supersaturations crystals had less perfection and higher misfit angles, and the distribution of angles was wider. In similar experimentation where the supersaturation is constant and crystals of different size were examined from the MSMPR, the mean misfit angle and standard deviation were higher at small crystal sizes and were both lower at large crystal sizes.

Nuclei were formed with a wide distribution of crystal perfection; the mean misfit angle or strain was higher for nuclei than for crystals occupying the larger sizes of the CSD. As a result, crystals with high levels of strain and low growth rates were washed out of the crystallizer leaving only crystals with low levels of strain and high growth rates to inhabit the upper size ranges of the CSD. If the strain was high, the crystal growth rate was slow, while if the strain was low, the crystal growth rate was rapid. This result can be seen in their experiments. Most potash alum crystals were nucleated with high levels of strain but it is only the crystals with low strain that grow fast enough to inhabit the product distribution and contribute significantly to its mass.

Dissertation Organization

The following three chapters are all papers that have been submitted or will soon be submitted for publication in different research journals. The first paper describes the experiments that explored the relationship of growth rate dispersion of secondary sodium nitrate nuclei to varying supersaturation conditions. The second paper attempts to further explain the results of the first paper and adds some additional results using potash alum and potassium sulfate. A growth rate model based upon strain and dislocations as determining factors in crystal growth is also developed. The third paper uses X-ray surface topography

and laser interferometry to look at the relationship between strain, dislocations, supersaturation, and growth rates. Following the three papers is a general conclusions section that ties together the main points and conclusions from the work presented in the three papers. It also identifies ideas for future work.

Nomenclature

Notation

A	area of a face
a	activity of solute
B	birth rate of crystals
B^o	birth rate of crystals at size=0
B_s	sample to film distance
c	concentration of solute
D	death rate of crystals
D_G	growth rate diffusivity
D_a	axial diffusivity
D_l	diffraction length
G	linear growth rate
h	step height
I	nucleation rate of critical size nuclei per unit area
J	mass flow of solute
k_c	mass transfer coefficient
L	crystal size or edge length
L'	radius of irradiated section
l	average size of mosaic blocks
M	radial asterism
N_T	Number of crystals
N_{Re}	Reynolds number
N_{Sh}	Sherwood number
N_{Sc}	Schmidt number
n	population density
n^o	population density at zero size
Q_i	volumetric flow rate of stream i
R	gas constant
S	undistorted diffraction dot size
S_B	supersaturation ratio
s^2	variance of distribution
T	temperature
t	time

t'	specimen thickness
V	crystallizer volume
z	distance in axial direction of plug flow crystallizer

Greek

ε	enhancement factor for due to dislocations
γ	activity coefficient
η	mosaic spread
μ	chemical potential
ν	number of ions per molecular unit
θ	Bragg angle of reflection
θ_m	mean misfit angle
ρ_c	size of a critical size nucleus
σ_a	dimensionless driving force using activities
σ_c	relative supersaturation
σ_l	BCF model term
τ	space time

Subscripts

eq	at equilibrium or saturation conditions

References

[1] Garside, J., "Industrial Crystallization from Solution," *Chemical Engineering Science*, **40**(1), 3(1985).

[2] Randolph, A. D., and M. A. Larson, *Theory of Particulate Processes*, Academic Press, New York (1971).

[3] Jones, A. G., J. Budz, and J. W. Mullin, "Crystallization Kinetics of Potassium Sulfate in an MSMPR Agitated Vessel," *AIChE Journal*, **32**(12), 2002(Dec. 1986).

[4] Girolami, M. W., and R. W. Rousseau, "Size-Dependent Crystal Growth-A Manifestation of Growth Rate Dispersion in the Potassium Alum-Water System," **31**(11), 1821(Nov.,1985).

[5] Ulrich J., "Growth Rate Dispersion-A Review," *Cryst. Res. Technol.*, **24**(3), 249(1989).

[6] Berglund, K. A., and M. A. Larson, "Modeling of Growth Rate Dispersion of Citric Acid Monohydrate in Continuous Crystallizers,"*AIChE Journal*, **30**(2), 280(March, 1984).

[7] Ramanarayanan, K. A., "Production and Growth of Contact Nuclei," Ph.D. Dissertation, Iowa State University, Ames, Iowa (1982).

[8] Berglund, K. A., E. L. Kaufman, and M. A. Larson, "Growth of Contact Nuclei of Potassium Nitrate," *AIChE Journal*, **29**(5), 867(Sept., 1983).

[9] Shanks, B. H., and K. A. Berglund, "Contact Nucleation from Aqueous Sucrose Solutions," *AIChE Journal*, **31**(1), 152(Jan., 1985).

[10] Mathis-Lilley, J. J., and K. A. Berglund, "Contact Nucleation from Aqueous Potash Alum Solutions," *AIChE Journal*, **31**(5), 865(May, 1985).

[11] Garside, J. and R. I. Ristic, "Growth Rate Dispersion Among ADP Crystals Formed by Primary Nucleation," *Journal of Crystal Growth*, **61**, 215(1983).

[12] Ramanarayanan, K. A., K. A. Berglund, and M. A. Larson, *Chemical Engineering Science*, **40**(8), 1604(1985).

[13] Ramanarayanan *et al.*, 1604.

[14] Girolami and Rousseau, 1821.

[15] Elankovan, P., and K. A. Berglund, *AIChE Journal*, **33**(11), 1844(1987).

[16] Teodossiev, N., *Journal of Crystal Growth*, **80**, 198(1987).

[17] Liang, B. M., R. W Hartel, and K. A. Berglund, "Growth Rate Dispersion in Seeded Batch Sucrose Crystallization," *AIChE Journal*, **33**(12), 2077(December, 1987).

[18] White, E. T., and P. G. Wright, "Magnitude of Size Dispersion Effects in Crystallization," *Chem Eng. Prog. Symp. Ser.*, **67**(110), 81(1971).

[19] Randolph, A. D., and E.T. White, "Modeling Size Dispersion in the Prediction of Crystal-Size Distribution," *Chemical Engineering Science*, **32**, 1067(1977).

[20] Tulke, A. and H. Offermann, " Measurement and Discussion of Potash Alum Crystal Growth Rate Fluctuations and Dispersion," *Journal of Crystal Growth*, **129**, 13(1993).

[21] Ramanarayanan, K. A., (1982).

[22] Berglund and Larson, 280.

[23] Garside, J. and R. I. Ristic, "Growth Rate Dispersion Among ADP Crystals Formed by Primary Nucleation," *Journal of Crystal Growth*, **61**, 215(1983).

[24] Zikic, A. M., R. I. Ristic, and J. N. Sherwood, "Three-parameter distribution function fit to growth rate dispersion among small crystals," *Journal of Crystal Growth*, **158**, 560(1996).

[25] Janse, A. H., and E. J. deJong, "Growth and Growth Dispersion," *Industrial Crystallization 78*, E. J. de Jong and A. H. Janse, Eds., North Holland Publishing Co., Amsterdam (1979).

[26] Berglund and Larson, 280.

[27] Larson, M. A., E. T. White, K. A. Ramanarayanan, and K. A. Berglund, "Growth Rate Dispersion in MSMPR Crystallizers," *AIChE Journal*, **31**(1), 90(Jan., 1985).

[28] Gupta, V., and S. K. Bhatia, "Growth Rate Dispersion in MSMPR Crystallizers: Solution by Regularization," *Chemical Engineering Science*, **48**(19), 3405(1993).

[29] Berglund, K. A., V. G. Murphy, *Ind. Eng. Chem. Fund.*, **25**, 174(1986).

[30] Zumstein, R.C., R. W. Rousseau, "GRD in Batch Crystallization with Transient Conditions," *AIChE Journal*, **33**(11), 1921(1987).

[31] Bohlin, M. and A. C. Rasmuson, "Modeling of Growth Rate Dispersion in Batch Cooling Crystallization,"*AIChE Journal*, **38**(12), 1853(1992).

[32] Girolami and Rousseau, 1821.

[33] Wang, S., A. Mersmann, and M. Kind, " Verification fo the Constant Crystal Growth Model for Attrition Particles and its Relevance to the modeling of Crystallizers," *Journal of Crystal Growth*, **99**, 1104(1990).

[34] Garside, J., "The Growth of Small Crystals," *Industrial Crystallization 78*, E. J. de Jong and A. H. Janse, Eds., North Holland Publishing Co., Amsterdam (1979).

[35] Berglund, Kaufman, and Larson, 867.

[36] Garside, 1979.

[37] Garside, J., and R. J. Davey, "Secondary Contact Nucleation: Kinetics, Growth and Scale-up," *Chem. Eng. Commun.*, **4**, 393(1980).

[38] Pamplin, B. R., ed., *Crystal Growth*, Pergamon, Oxford (1980).

[39] Mullin, J. W., *Crystallization*, Butterworth and Co., Ltd., London (1972).

[40] Strickland-Constable, R. F., *Kinetics and Mechanisms of Crystallization*, Academic Press, New York, NY (1968).

[41] Ohara, M. and R. C. Reid, *Modeling Crystal Growth Rates from Solution*, Prentice-Hall Inc., Englewood Cliffs, N. J. (1973).

[42] Hartman, P., ed., *Crystal Growth: an Introduction*, North Holland, Amsterdam (1973).

[43] Benema, P., *Industrial Crystallization*, Mullin, J. W., ed., Plenum Press, New York, NY (1976).

[44] Ohara, M. and R. C. Reid, 1973.

[45] *Ibid.*, 1973.

[46] *Ibid.*, 1973.

[47] Burton, W.K., N. Cabrera, and F. D. Frank, "The Growth of Crystals and the Equilibrium Structure of Their Surfaces," *Phil. Trans. Roy. Soc.*, **243**, 299(1951).

[48] Chernov, A. A., *Soviet Physics Uspekhi*, **4**(1),116(1961).

[49] Bennema, P., Spiral Growth and Surface Roughening: Developments Since Burton, Cabrera, and Frank," Journal of Crystal Growth, 69, 182(1984).

[50] Garside, J., " The Role of Transport Processes in Crystallization,"*Advances in Industrial Crystallization*, Butterworth Heinemann, Oxford (1991).

[51] Garside, J., and R. J. Davey, "Secondary Contatct Nucleation: Kinetics Growth and Scale-Up," *Chem. Eng. Commun.*, **4**, 393(1980).

[52] Valcic, A. V., *Journal of Crystal Growth*, **30**, 129(1975).

[53] Davey, R. J., R. I. Ristic, and B. Zizic, *Journal of Crystal Growth*, **47**, 1(1979).

[54] Harris, S. "A Microscopic Kinetic Theory of Crystal Growth," *Journal of Crystal Growth*, **97**, 319(1989).

[55] Ristic, R. I., J. N. Sherwood, and T. Shripathi, "The Role of Dislocations and Mechanical Deformation in Growth Rate Dispersion in Potash Alum Crystals," *Advances in Industrial Crystallization*, Butterworth Heinemann, Oxford (1991).

[56] Ristic, R. I., J. N. Sherwood, and T. Shripathi, "The Role of Dislocations and Mechanical Deformation in Growth Rate Dispersion in Potash Alum Crystals," *Advances in Industrial Crystallization*, Butterworth Heinemann, Oxford (1991).

[57] Human, H. J., W. J. P. van Enckevort, and P. Bennema, "Spread in Growth Rates of the {111}, {100} and {110} Faces of Potash Alum Growing from Aqueous Solution," *Industrial Crystallization 81*, S. J. Jancic and E. J. de Jong Eds., North-Holland Publishing Co., Amsterdam(1982).

[58] Ristic, R. I., J. N. Sherwood, and T. Shripathi, "The Role of Dislocations and Mechanical Deformation in Growth Rate Dispersion in Potash Alum Crystals," *Advances in Industrial Crystallization*, Butterworth Heinemann, Oxford (1991).

[59] Ristic, R. I., J. N. Sherwood, and T. Shripathi, (1991).

[60] Bhat, H. L., R. I. Ristic, J. N. Sherwood, and T. Shripathi, "Dislocation Characterization in Crystals of Potash Alum Grown by Seeded Solution Growth Under Conditions of Low Supersaturation," *Journal of Crystal Growth*, **121**, 709(1992).

[61] Ristic, R. I., J. N. Sherwood, and T. Shripathi, "The Role of Dislocations and Mechanical Deformation in Growth Rate Dispersion in Potash Alum Crystals," *Advances in Industrial Crystallization*, Butterworth Heinemann, Oxford (1991).

[62] Ristic, R. I., B. Shekunov, and J. N. Sherwood, "Long and Short Period Growth Rate Variations in Potash Alum Crystals," *Journal of Crystal Growth*, **160**, 330(1996).

[63] Ristic, R. I., J. N. Sherwood, and T. Shripathi, "The Role of Dislocations and Mechanical Deformation in Growth Rate Dispersion in Potash Alum Crystals," *Advances in Industrial Crystallization*, Butterworth Heinemann, Oxford (1991).

[64] Ristic, R. I., J. N. Sherwood, and K. Wojciechowski, "Assessment of the Strain in Small Sodium Cholorate Crystals and its Relation to Growth Rate Dispersion," *Journal of Crystal Growth*, **91**, 163(1988).

[65] Ristic, R. I., J. N. Sherwood, and T. Shripathi, "The Role of Dislocations and Mechanical Deformation in Growth Rate Dispersion in Potash Alum Crystals," *Advances in Industrial Crystallization*, Butterworth Heinemann, Oxford (1991).

[66] Van der Heijden, A. E. D. M. and J. P. van der Eerden, "Growth Rate Dispersion: the Role of Lattice Strain," *Journal of Crystal Growth*, **118**, 14(1992).

[67] Ristic, R. I., J. N. Sherwood, and K. Wojciechowsky, 163.

[68] Ristic, R. I., J. N. Sherwood, and T. Shripathi, 1991.

[69] A. E. D. M. van der Heijden, M. Elwenspoek and J. P. van der Eerden, *Journal of Crystal Growth*, **98**, 398(1989).

[70] Zacher, U. and A. Mersmann, "The Influence of Internal Crystal Perfection on Growth Rate Dispersion in a Continous Suspension Crystallizer," *Journal of Crystal Growth*, **147**, 172(1995).

[71] van der Heijden, A. E. D. M. and J. P. van der Eerden, "Growth Rate Dispersion: the Role of Lattice Strain," *Journal of Crystal Growth*, **118**, 14(1992).

CHAPTER 2. CHARACTERIZING GROWTH RATE DISPERSION OF $NANO_3$ SECONDARY NUCLEI AS A FUNCTION OF SUPERSATURATION

A paper submitted for publication in *AIChE Journal*

Christopher M. Jones[1] and Maurice A. Larson

Abstract

The purpose of this work was to characterize sodium nitrate secondary nuclei growth rate dispersion as a function of the supersaturation conditions present during nucleation and growth. Two methods producing two sets of data were recorded. The first set included examining the response of the growth rate distributions at four different supersaturations. The second set of data examined the response surface of growth rate dispersion (GRD) parameters where the supersaturation at nucleation and during growth were both altered. GRD causes deviations from the theoretical crystal size distribution predicted by the population balance. The most visible effect of GRD is the presence of more crystals in the small size range than is predicted by theory for mixed-suspension mixed-product removal continuous crystallizers. GRD is a key factor in determining how various crystallization systems operate. The growth rates of nuclei determine the number of crystals that will grow large enough to populate the upper sizes of the crystal size distribution and contribute to the final product mass.

---

1 Please Contact Christopher Jones in Correspondence for this Paper

Introduction

Growth rate dispersion (GRD) was first recognized as a phenomenon having a serious bearing on crystallizer performance in 1971 by White and Wright (1971). They observed that the standard deviation of an initially narrow size distribution of crystals in a batch crystallizer increased as time progressed. Thus, the growth rates could not all be the same for all crystals.

Early work performed on the GRD phenomenon first centered on defining and clarifying how GRD manifested itself in crystallization systems. A particular point of emphasis was the question of whether the growth rates of crystals fluctuated randomly, the random fluctuation (RF) model, (Randolph and White, 1976) or whether they were constant for each crystal, the constant crystal growth (CCG) model (Ramanarayanan, 1982), where the growth rates of all the crystals in a system could be fit by a probability density distribution. Further work assuming the CCG model has shown how the growth rate distribution of crystals in a mixed-suspension mixed-product removal (MSMPR) crystallizer can be derived from the product size distribution (Larson, *et al.*, 1985). Recent work has virtually dismissed the notion of the RF model of GRD in favor of an intrinsic growth rate (IGR) model. The proposed IGR model assumes that a crystal's growth rate does not fluctuate randomly but is intrinsic to each crystal in the system and may change as system parameters change. At any time during the crystallization process, the growth rates of crystals in the crystallizer system may be expressed as a growth rate distribution.

While these research projects have helped define what facet of crystal behavior causes GRD, virtually no work has been performed that investigating how GRD is affected by system parameters such as supersaturation, stirring speed, or slurry density. No criteria has

been established for defining GRD for a particular system. To remedy that situation, the accepted idea that crystal growth rates are intrinsic and may be fit by a probability distribution is used. Thus, defining the GRD of a system requires parameterizing the growth rate distribution, specifically in terms of its mean, standard deviation, coefficient of variation, and its symmetry.

It is the growth rates of nuclei that determine the final product size distribution of a crystallizer. If a crystal nucleus is slow growing, it will be washed out of the crystallizer before ever reaching a size large enough to contribute significantly to the final product mass. Furthermore, in most crystallization systems nucleation is occurring at supersaturations much less than those required to initiate primary nucleation. It is well known that secondary nucleation occurs at low levels of supersaturation. Thus, to determine how real system GRD is effected by system changes, secondary nuclei must be the focus of attention.

The purpose of the work presented in this paper is to characterize the GRD of secondary $NaNO_3$ nuclei as a function of supersaturation. Supersaturation is a defining element in crystal growth and nucleation theory. The development of a working knowledge that describes the relationship of GRD with respect to supersaturation will be helpful in a pragmatic sense and in choosing new directions of crystallization research.

Experimental

Growth Cell

The growth rates of secondary nuclei produced and grown under various levels of supersaturation were monitored. The cell used for secondary nucleation and growth was similar to that developed and used by Garside and Larson (1978) and is shown in Figure 2.1.

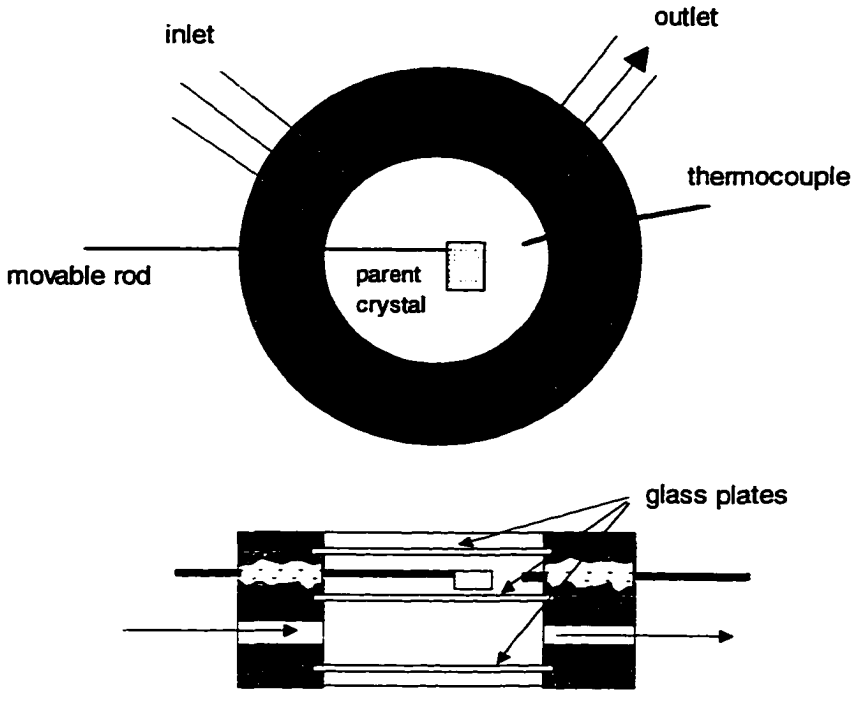

Figure 2.1 Schematic of the growth cell used to observe secondary nuclei

The cell had two chambers and consisted of four stainless steel sections. The sections were separated by glass plates for the transmission of light from a microscope. Neoprene O-rings sealed the cell against fluid loss. The lower chamber had a volume of 8 ml, and it had an inlet and an outlet for the circulation of water from a Fisher Model 80 constant temperature circulator. The upper chamber held the saturated solution and had a volume of 5 ml. The upper chamber also contained a thermocouple and the parent crystal mounted on a stainless steel rod.

A Nikon Optiphot-2 microscope was used in coordination with a Javelin black and white digital video camera mounted on the microscope. Using a Coreco Oculus TCX/MX Frame Grabber and a Sony SVO-9500 MD VHS recorder, a run was taped for later image

analysis. Image analysis was performed using Image Pro. Images were captured from the Fuji T-160 VHS tape and the sizes of various nuclei were recorded.

Constant temperature circulators were used to control the temperature of the cell. Nalgene tubing connected the water baths to the cell, and valves were used to control the flow from various constant temperature baths.

Materials and Procedure

Saturated Solution. Analytical grade $NaNO_3$ and distilled water were used to make the saturated solution. After mixing with a magnetic stirrer in an Erlenmeyer flask, the flask was put in a water bath at the desired temperature making sure that a large excess of solid crystal still existed in the solution. The solution was considered saturated after having been in the bath for 5 days with excess crystal. Sodium nitrate was used for this work because it was easy to identify and measure the crystallographic faces.

Parent crystals were prepared by allowing saturated solution of the desired substance to evaporate over many days. Crystals were nucleated by primary nucleation. When the growing crystals reached about 4-10 mm long, they were removed from the solution and dried. The parent crystal was mounted in the cell using fast setting epoxy to glue it to the movable stainless steel rod.

Procedure. At the beginning of any run, the cell was preheated with water from one of the circulating water baths to a temperature about 1 °C greater than the saturation temperature. This ensured that when saturated solution was added to the cell that it did not undergo primary nucleation. The cell was mounted on the stage of the microscope so that its position could be manipulated mechanically. Five ml of saturated solution was withdrawn

from the flask and transferred to the upper chamber of the cell. Then, a glass plate was put over the upper chamber to prevent evaporation and to facilitate using the microscope. Using the microscope, the upper chamber was examined to determine whether any nucleation had occurred or if some other contamination existed forcing the experiment to be stopped and restarted.

Once the existence of nuclei in the cell was shown to be negative, the flow of circulating water was changed to a second water bath with a lower temperature. Thus, the solution became supersaturated and the parent crystal endured a change from a dissolving environment to a growing environment.

When the temperature of the cell had reached steady state, the parent crystal was contacted by sliding it 2 cm across the glass plate. Contact nuclei were formed by this event. The progress of the run was recorded using a VHS recorder. Recording was started two seconds before the parent crystal was contacted. The cell temperature was recorded at intervals throughout the run.

Two sets of experiments were performed. The first set examined the GRD of specific faces of $NaNO_3$ when the supersaturation during nucleation and growth were the same. The second set of experiments examined the GRD of a characteristic dimension when the supersaturation during nucleation and growth were varied.

Measurements. Secondary nuclei were examined and crystals were not selected for analysis if they exhibited any of the following:

- One whole edge was touching another crystal.
- It could not be distinguished from surrounding crystals.

- It appeared to be the joining of two smaller crystals.

The Miller indices for the sodium nitrate faces are given in Figure 2.2. The sodium nitrate crystal habit is a rhombahedron, thus a parallelepiped, which makes for the easy identification and measurement of specific crystallographic faces. In the first set of experiments the GRD of specific faces was compared.

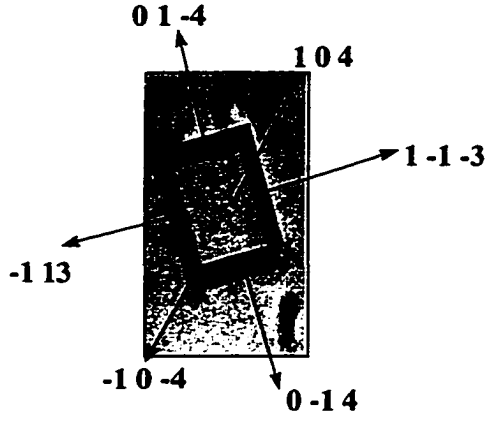

Figure 2.2 Miller indices for $NaNO_3$, a trigonal(hexagonal) system

Using Image Pro, the size of a characteristic dimension--the square root of the area of the 104 or $\bar{1}\bar{0}\bar{4}$ face was measured and plotted with respect to time for selected crystals. Excel and JMP were used for data reduction and plotting various regression models.

In the first set of experiments the growth rate distributions of the 113 face, the 014 face, and the characteristic dimension were determined, but only the data from the characteristic dimension analysis are included here. In the second set of experiments only the characteristic dimension was studied.

Experimental Parameters. The relative supersaturation, σ, for any given set of experimental conditions was determined by using a plot of the solubility of sodium nitrate in water with respect to temperature. The relative supersaturation is found using Equation 1,

$$\sigma = \frac{C - C_{eq}}{C_{eq}} \tag{2.1}$$

where C is the concentration of the supersaturated solution in units of (g $NaNO_3$/100 g H_2O) and C_{eq}, with the same units, is the equilibrium concentration of the solution at the given temperature.

Experiment Set #1. In experiment set #1 only one experimental variable existed, the supersaturation of the system, because the supersaturation present during nucleation and growth was the same. Table 2.1 shows the level of under-cooling and the associated relative supersaturation for each run performed in Set #1. The initial growth rates of the characteristic dimension for 3181 nuclei were measured in this set.

Table 2.1 Supersaturation conditions for experimental set #2

Run #'s	ΔT °C	σ=(C-Ceq)/Ceq	# Crystals Measured
1-2	3.3	0.028	428
3-5	4.3	0.037	679
6-8	5.2	0.045	783
9-11	6.3	0.054	1291

For each set of conditions, the growth rate distributions of three dimensions were compared: the characteristic length, the 113 face, and the 014 face.

Experiment Set #2. This experiment was designed to de-couple the effect of supersaturation at nucleation and during growth. Since the results of set #1 showed non-linear behavior in some of the response variables, it was thought that the second set of

experiments should also allow for the detection of non-linearity. To meet that end a response surface experiment was designed and carried out. Response surface experiments allow the analysis of curvature in a surface defined by two experimental parameters. In all cases, statistical significance was set to be at the 99% confidence level.

Relative supersaturation was determined the same way as in Set #1, where the concentration is defined in units of (g $NaNO_3$/100 g H_2O). The relative supersaturations were then coded; this allowed for statistical analysis without the possibility of collinearity between terms. The coded supersaturation was defined as,

$$X_{1,2} = \frac{2\bullet(\sigma-0.041)}{0.026} \tag{2.2}$$

X_1 is the coded supersaturation at nucleation and X_2 is the coded supersaturation used when the crystal is growing. The coding was devised such that when X=1 the relative supersaturation corresponds with the highest level of supersaturation used in Set #1, σ=0.054, and when X=-1 the relative supersaturation corresponds with the lowest level of supersaturation used in Set #1, σ=0.028

The response surface design is shown in Table 2.2. The experiment included the measurement of the initial growth rates of 187 nuclei. Both the mean and the standard deviation of the the initial growth rate distributions were analyzed to determine their responses to X_1 and X_2.

However, the mean and standard deviation are analyzed differently. Because a distribution of standard deviations is skewed, the log of the standard deviation was fit. Taking the log of the standard deviation maps the skewed distribution into a form resembling a normal distribution. This allows for the correct statistical analysis, since detecting the

statistical significance of a statistic is based upon the assumption that the statistic is normally distributed.

Table 2.2 Experiment set #2 response surface design

Pattern	X_1	X_2	# Crystals Measured
--	-1	-1	20
+-	1	-1	20
-+	-1	1	20
++	1	1	20
-0	-1.41	0	20
+0	1.41	0	20
0-	0	-1.41	20
0+	0	1.41	20
00	0	0	27

Results

While determining the growth rates of nuclei, it became immediately apparent that the growth rate changed as time progressed. That is, the measurements of nuclei plotted with respect to time did not yield a linear fit in most cases. Instead the growth rate decelerated as time progressed. Regardless of the cause of this phenomenon, it forced the fitting of a quadratic equation to the relationship between size and time, Equation 2.3.

$$S = at^2 + bt + c \tag{2.3}$$

The growth rate at any time could then be found by taking the first derivative Equation 2.3, Equation 2.4.

$$G = 2at + b \tag{2.4}$$

Since the interest is on describing the GRD behavior of nuclei, we are interested in the growth rate distributions at the time closest to the nucleation event, where t=0. Thus,

when we describe the GRD of nuclei in terms of the initial growth rate distribution; in the case of this analysis it becomes a distribution of the fitted parameter, b.

Experiment Set #1. The first set of experiments shows that the predicted response of the mean of the initial growth rate distribution with respect to supersaturation is non-linear. In this case the supersaturation at nucleation and during growth are the same. This is equivalent in the second experiment to setting X_1 and X_2 to be equal to each other.

The initial growth rate distributions fit a gamma distribution. This is a skew right distribution. Figure 2.3 shows the jittered distributions of the initial growth rates of the characteristic length of crystals by varying relative supersaturation. A line connects the means and the boxes surrounding the data points are quantile boxes. The jittering effect along with the quantile boxes are useful for getting a feel for the distribution shape at each set of experimental conditions.

Comparing the initial growth rate distributions of specific faces at each set of conditions shows that there is no difference between the initial growth rate distributions of the 113 face, the 014 face, or the characteristic length. This is as expected since the faces of sodium nitrate are crystallographically equivalent. It is for this reason that only the data from the characteristic length are presented and only the characteristic length was studied in set #2.

Statistical analysis of the data in Figure 2.3 results in the following predictive equations for the mean and standard deviation of the initial growth rate distribution:

$$\mu = -0.514 + 36.3\sigma - 405\sigma^2 \tag{2.5}$$

$$\sigma_{IG} = \exp(-3.49 + 26.4\sigma) \tag{2.6}$$

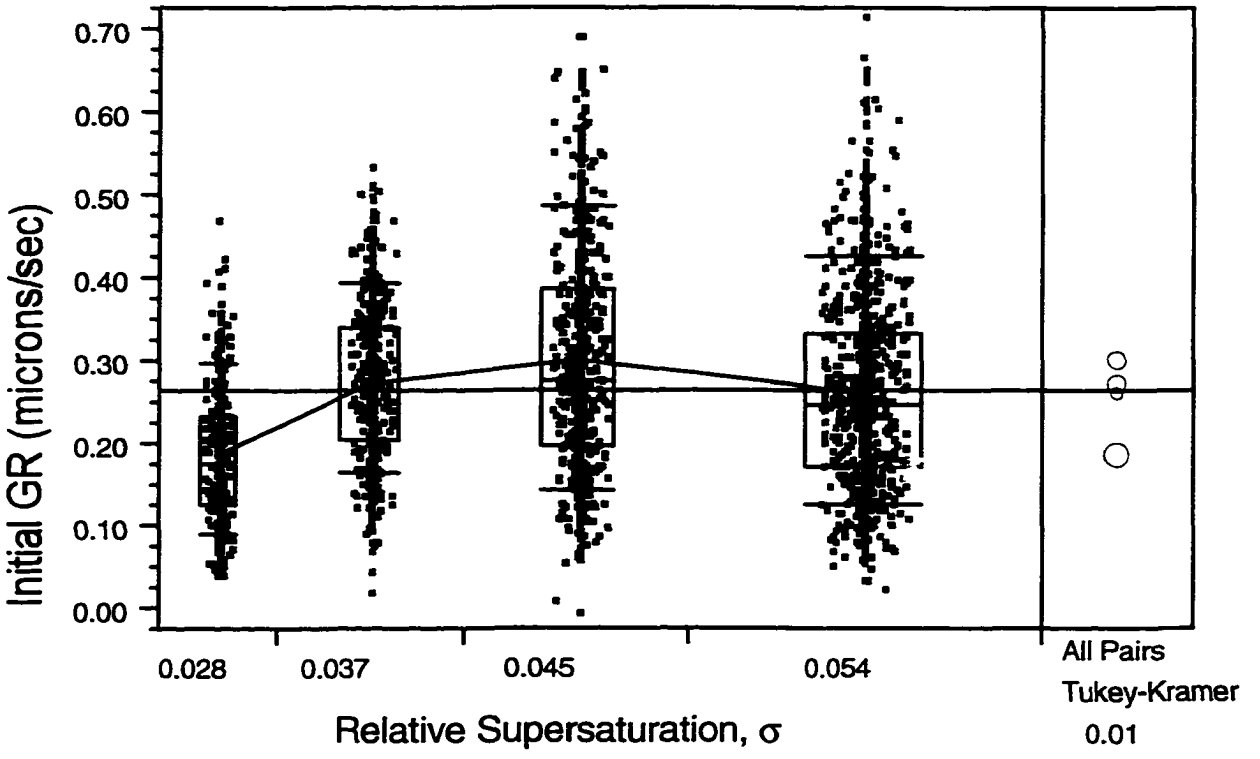

Figure 2.3 Set #1 results showing the initial growth rates at varying relative supersaturations

Equation 2.5 predicts and Figure 2.3 shows that the response of the mean passes through a maximum. The response of the standard deviation in Equation 2.6 increases with increasing supersaturation.

The standard deviations were fit using the log of the standard deviation because the distribution of standard deviations is skewed, a Chi distribution. To normalize a skewed distribution and allow the correct statistical analysis, it is necessary to analyze the log of the parameter. The standard deviation of the initial growth rate distribution increases as the supersaturation increases.

The coefficient of variation (CV), which passes through a minimum, is a measure of the relative spread of the growth rate distribution, can be determined by dividing the standard deviation, Equation 2.6, by the mean, Equation 2.5, in Equation 2.7.

$$CV = \frac{\sigma_{IG}}{\mu} \tag{2.7}$$

Experimental Set #2. In Figure 2.4 the response surface of the mean initial growth rate is plotted on a contour plot with respect to σ_1 and σ_2, the relative supersaturations at nucleation and growth. The lines of the contour plot represent different values of the mean. The surface has a saddle point. The behavior of the mean of the initial growth rate distribution is highly dependent upon both σ_1 and σ_2. Thus, changing the supersaturation conditions present during nucleation can drastically alter the GRD behavior of the system.

The response surface analysis yielded the following models, in terms of the relative supersaturations σ_1 and σ_2, for the mean and standard deviation of the initial growth rate distribution after dropping statistically insignificant terms:

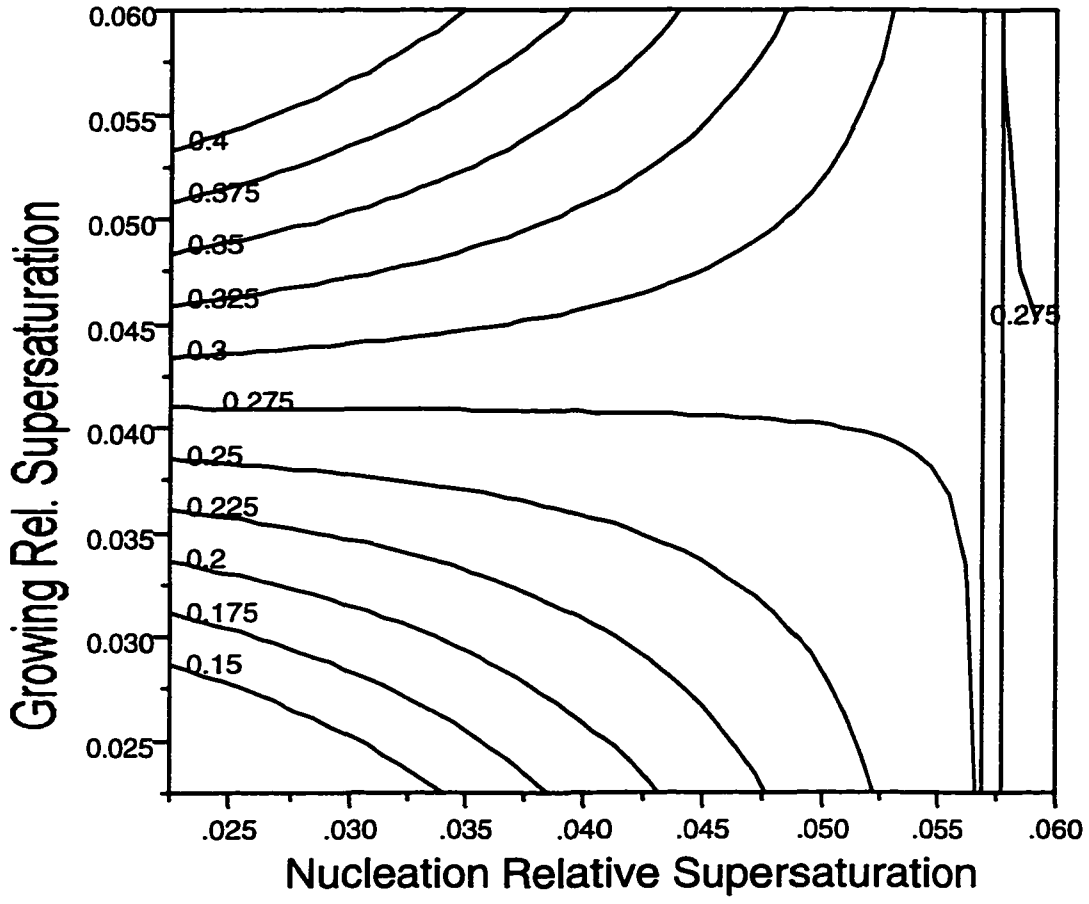

Figure 2.4 Contour plot of the mean of the initial growth rate distribution as a function of relative supersaturation at nucleation, σ_1, and during growth, σ_2

$$\mu = -0.415 + 16.8\sigma_2 - 292.\sigma_1\sigma_2 + 12.08\sigma_1 \tag{2.8}$$

$$\sigma_{IG} = \exp(-3.39 + 24.6\sigma_2) \tag{2.9}$$

and again the CV can be calculated as in Equation 2.7.

The model of the standard deviation is dependent only upon the supersaturation present during growth, σ_2. The relationship between growing supersaturation and the standard deviation is displayed in Figure 2.5. The line represents the modeled equation and the points are experimental points.

Figure 2.6 shows the response of the coefficient of variation of the initial growth rate distribution to σ_1 and σ_2 on a contour plot. Each line represents a different value of CV. The surface has a saddle point. The behavior of the CV is similar to that of the mean in that it is highly dependent upon both the nucleation and growing supersaturations. Altering the nucleation supersaturation can greatly alter the response of the CV to the growing supersaturation.

Comparing the Results of Set #1 and Set #2. By setting both σ_1 and σ_2 to be equal, the models derived in the analysis of set #2 for the mean, standard deviation, and CV of the initial growth rate distribution can be compared to the models of set #1 as shown in Figure 2.7.

The error bars are calculated using $\pm 3\times$ (standard error), providing 99% confidence intervals for the fitted curves. The plots show there is good agreement between the two sets of experiments for the mean, standard deviation, and the CV.

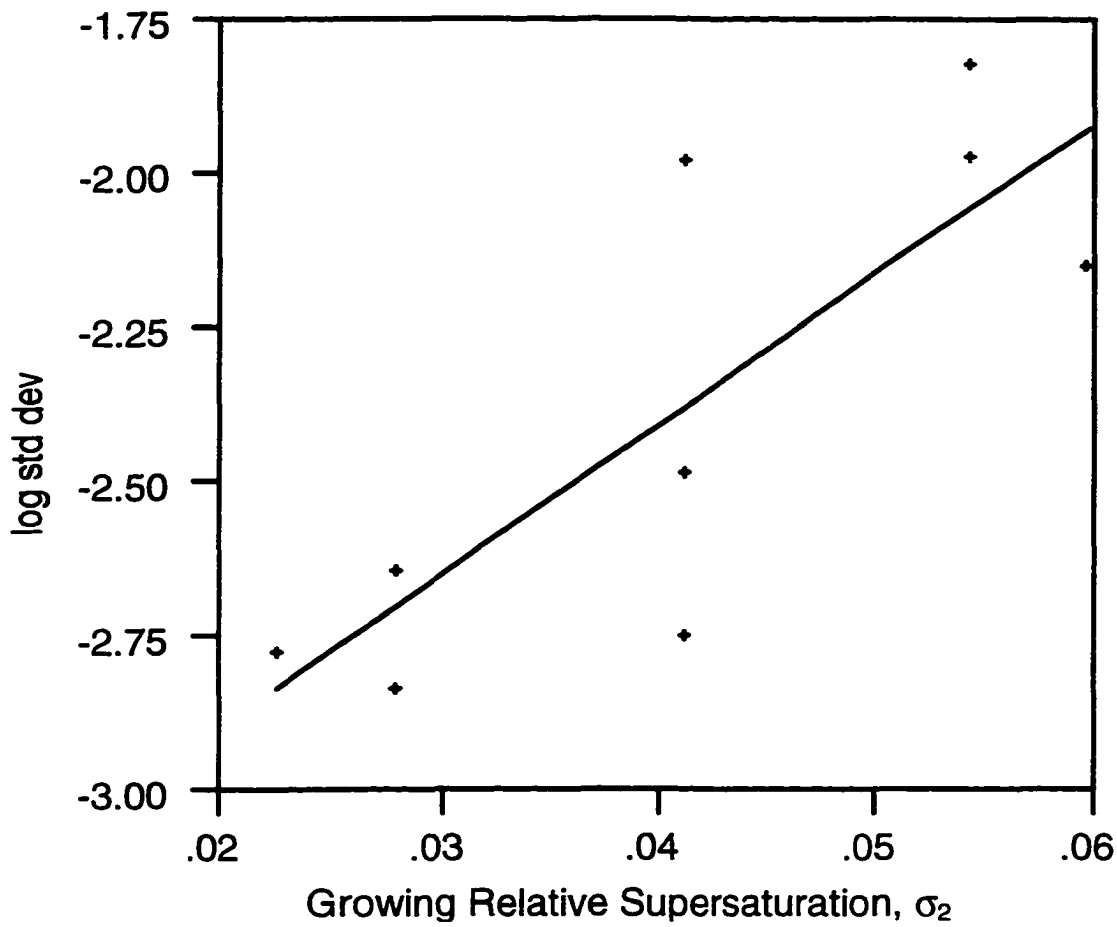

Figure 2.5 Plot of the log (standard deviation (microns/sec) of initial growth rate distribution) with respect to the relative supersaturation during growth

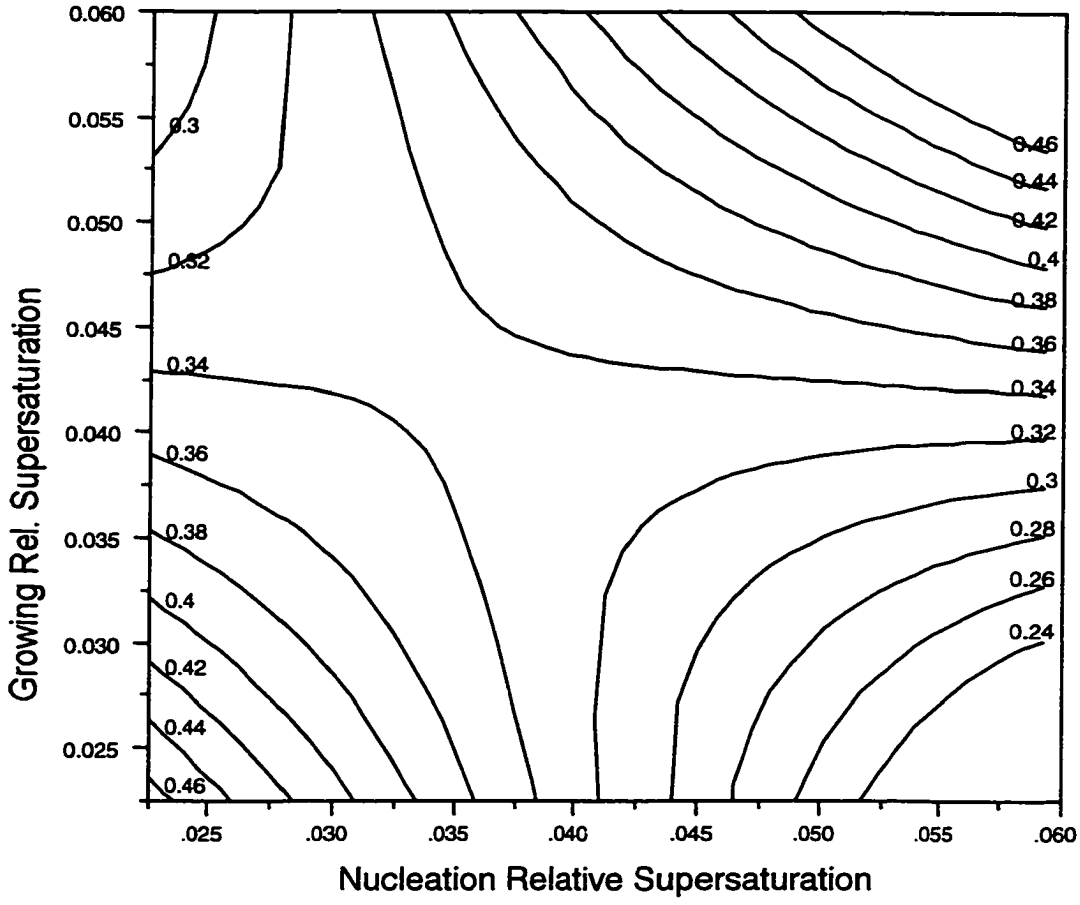

Figure 2.6 Contour plot of the coefficient of variation, CV, with respect to the relative supersaturation at nucleation, σ_1, and during growth, σ_2

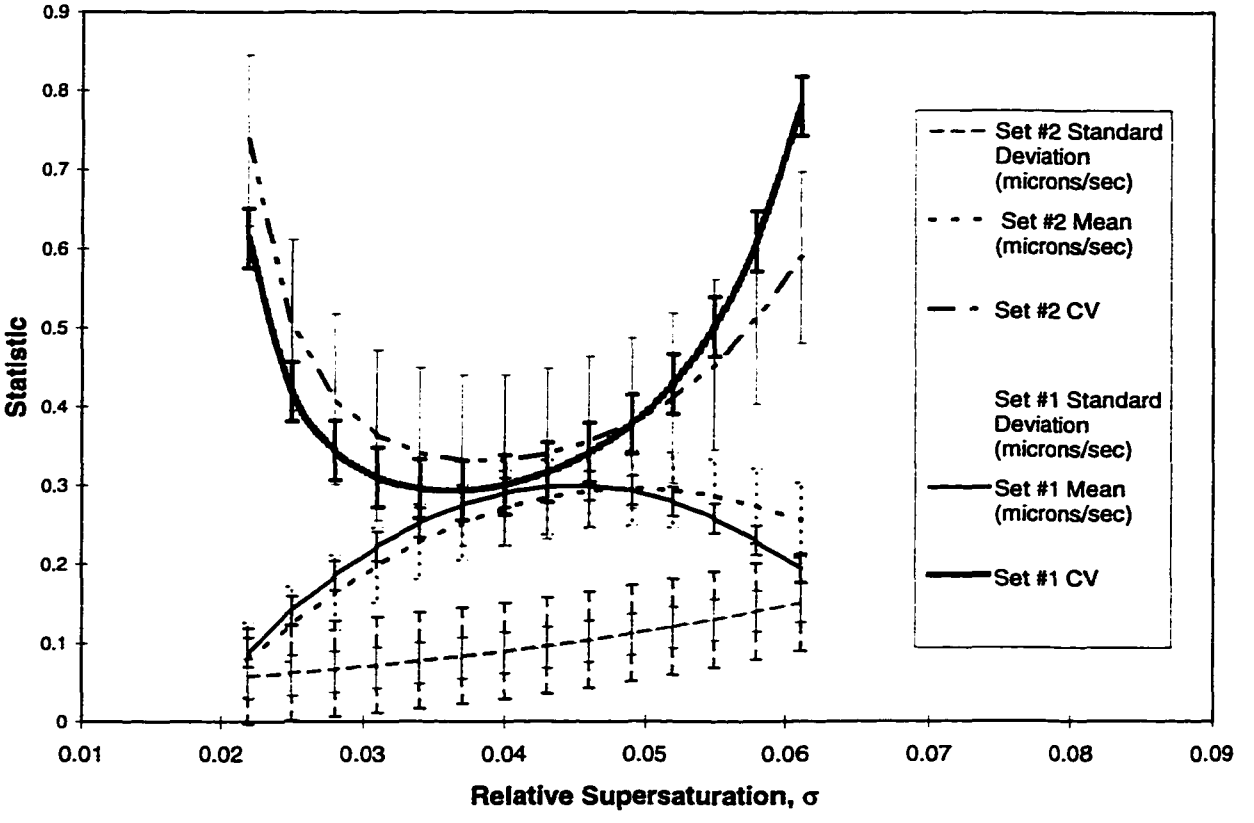

Figure 2.7 Comparison of the predicted response of the mean, standard deviation, and CV when the supersaturation at nucleation and during growth are the same for experiment sets #1 and #2

Discussion

Experiment set #1 showed that the initial growth rate distribution can be fit very well by a gamma distribution. In addition, comparisons of the initial growth rate distributions of the characteristic length, the 113, and 014 faces showed that there was no detectable difference between them. This was as expected because the faces of sodium nitrate are crystallographically equivalent.

Experiment set #1 showed that the standard deviation of the initial growth rate distribution increased with increasing supersaturation, while the response of the mean passed through a maximum. This was curious behavior that is later accounted for in the results of experiment set #2. The response of the mean was a result of a more complicated dependency of the initial growth rate distribution upon the supersaturation conditions at nucleation and during growth.

In experiment set #2 the response of the standard deviation of the initial growth rate distribution mimicked the behavior in set #1. The relationship of the standard deviation to supersaturation was clarified however, as the analysis of set #2 showed that the standard deviation was dependent only upon the supersaturation present during growth. Changing the nucleation supersaturation had no effect on standard deviation.

In contrast, the mean of the initial growth rate distribution was shown to be a strong function of both the nucleation and growing supersaturations. The behavior of the mean on the response surface was highly dependent upon what region of the response surface was being examined. Examining specific slices of the mean's response surface provides a way of

clarifying and separating trends of the response surface with respect to specific forces which are known to effect crystal growth.

Figure 2.8 shows the response of the mean of the initial growth rate distribution with respect to increasing nucleation supersaturation at two levels of growing supersaturation. The mean increases with respect to increasing nucleation supersaturation at the low level of growing supersaturation.

The mean decreases at the high level of growing supersaturation. This indicates two separate regions of control. The first region being dislocation controlled and the second region being strain controlled. Strain and dislocation both occur simultaneously in the crystal. Strain being a natural result of having dislocations. However, strain and dislocations have opposite effects on crystal growth rates. Ristic, *et al.* (1991) working with macro sized potash alum crystals showed that increasing dislocation density results in increasing crystal growth rates. In separate experiments they showed that increasing strain in macro sized potash alum crystals decreases the growth rates of the crystals. In addition, if the strain reached a critical level, the growth of the crystal could be stopped entirely until either the strain was released or the supersaturation was changed.

Zacher and Mersmann (1991) showed in MSMPR experiments using potash alum that increasing the level of supersaturation in the crystallizer increased the level of strain and imperfections in the alum crystals. In addition, large crystals or those with high growth rates had the lowest levels of strain, while small crystals had the highest levels of strain. These results support the findings of Ristic *et al.* that strain causes crystals to grow slowly while

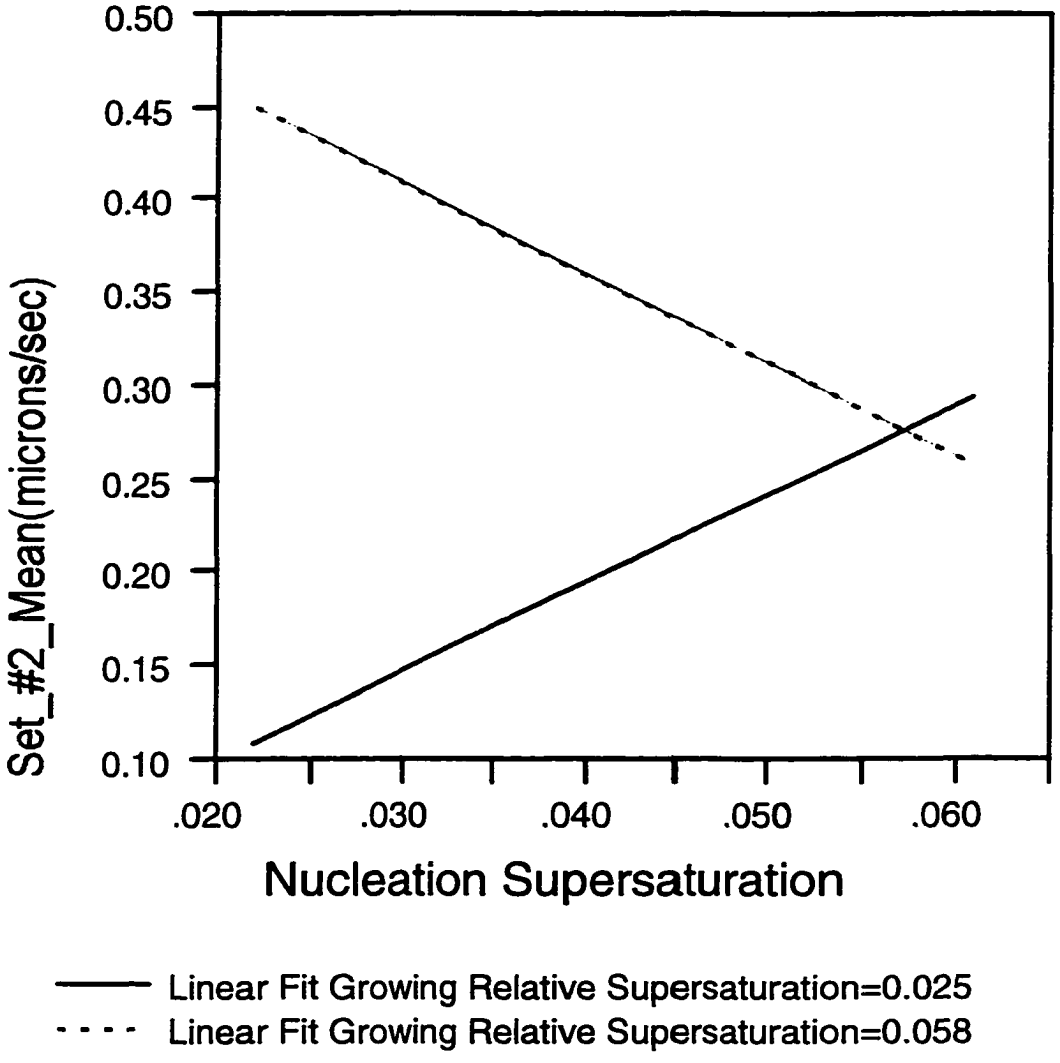

Figure 2.8 Response of the mean initial growth rate with respect to nucleation supersaturation at two levels of growing supersaturation

low levels of strain allow crystals to grow more rapidly while asserting that high levels of supersaturation increase the level of strain in crystals.

Figure 2.9 shows the response of the mean of the initial growth rate distribution with respect to increasing growing supersaturation at two levels of nucleation supersaturation. The mean increases with respect to increasing growing supersaturation at the low level of nucleation supersaturation. It remains relatively constant at high levels of nucleation supersaturation. These results suggest that at low levels of nucleation supersaturation, relatively low levels of dislocations and strain are created. At a high level of nucleation supersaturation, high level of dislocations and strain are created. The results show that at low levels of strain changing the growing supersaturation will have an effect on the growth rates of crystals in the system. At a critical level of nucleation supersaturation, the dislocation structure becomes such that changes in the growing supersaturation will have little effect on the crystal growth rates as the bulk effect of strain has become the controlling force dictating the growth rates.

It should also be noted that when comparing the results of set #1 and set #2 that the results match up very well with one another. The response of the standard deviation is almost the same. The modeled response of the mean for both sets predicts that a maximum will occur. This maximum being a result of the complicated dependency of the mean upon both the nucleation and growing supersaturations.

The CV or relative spread is an indication of comparing the spreads of distributions with different means. The coefficient of variation for both sets passes through a minimum and match up well with one another. It is also worth noting that set #1 and set #2 were

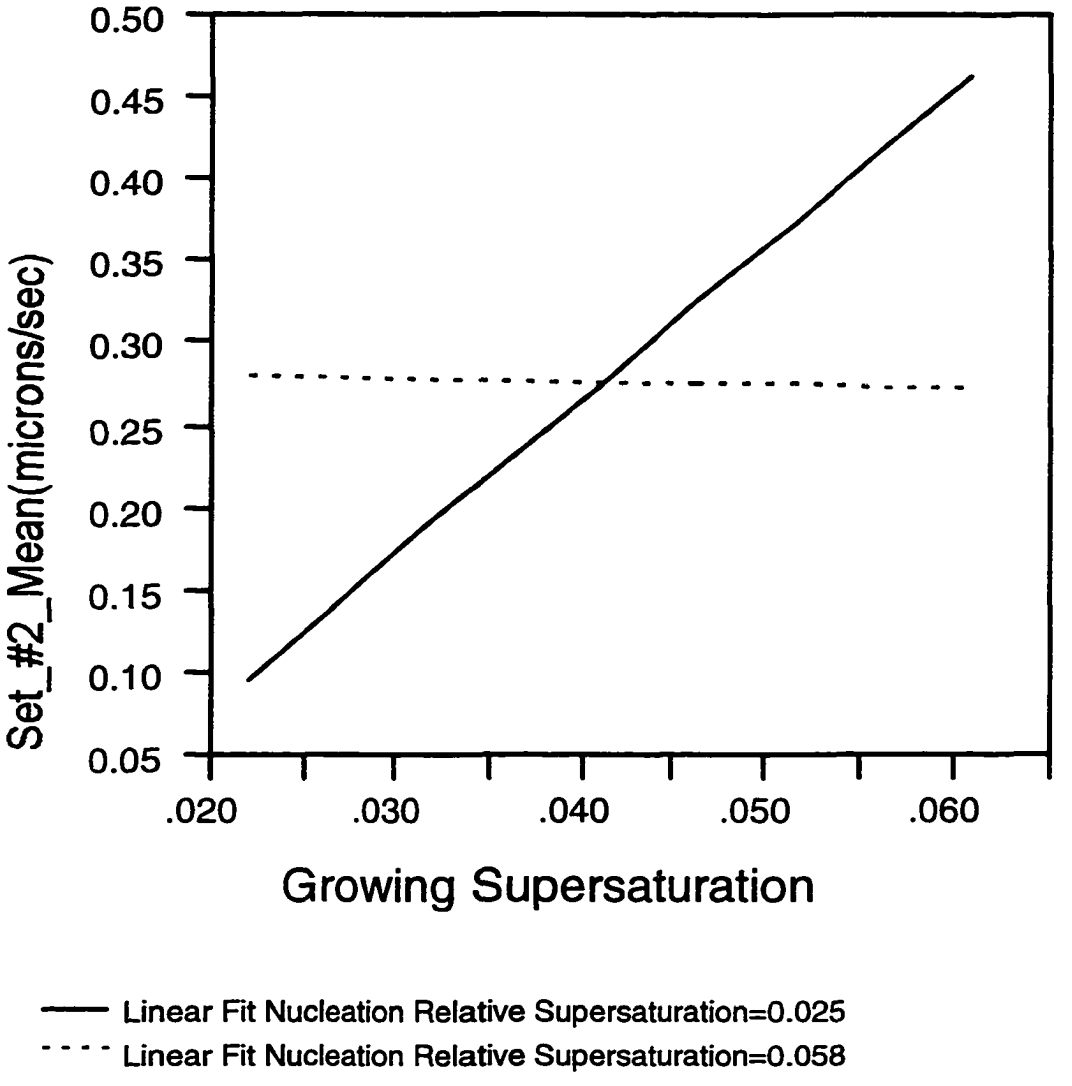

Figure 2.9 Response of the mean initial growth rate with respect to growing supersaturation at two levels of nucleation supersaturation

performed a year and a half apart from one another. The crystal measurements were performed by two different individuals. And the number of crystals examined in the two experiments was different by about 3000 crystals. Still, the results match up very well.

Conclusions

The initial growth rate distribution is fit well by a gamma distribution. The response of the mean, standard deviation, and the CV of the initial growth rate distribution have been found with respect to the supersaturation during nucleation and growth. The mean and coefficient of variation of the initial growth rate distribution are dependent upon both the supersaturation at nucleation and the supersaturation during growth. The standard deviation of the initial growth rate distribution is dependent only upon the supersaturation present during growth.

The results are reproducible. The two sets of experiments were performed one and half years apart with the measurements performed by two different people. The general trends of the mean and standard deviation of the initial growth rate distribution are displayed in Table 2.3.

Table 2.3 Trends of the initial growth rate distribution with varying conditions of supersaturation.

Nucleation Supersaturation	Growing Supersaturation	Initial Growth Rate Mean	Initial Growth Rate Standard Deviation
Increases	Increases	Varies	Increases
Increases	Decreases	Varies	Decreases
Decreases	Fixed	Increases	Constant
Fixed	Decreases	Varies	Decreases

Acknowledgments

The authors are grateful to Wayne Genck of Genck International for his financial support and to Seth Holmen who worked as an undergraduate research assistant on experiment set #1.

Nomenclature

C Concentration of sodium nitrate in solution(g $NaNO_3$/ 100 g H_2O)

C_{eq} Equilibrium concentration of sodium nitrate in solution (g $NaNO_3$/ 100 g H_2O)

X Coded relative supersaturation

S Characteristic length (microns)

G Growth rate of the characteristic length (microns/second)

t Time (seconds)

CV Coefficient of Variation

Greek Symbols

σ Relative supersaturation

μ Mean of the initial growth rate distribution

σ_{IG} Standard deviation of the initial growth rate distribution

Subscripts

1 At nucleation

2 During growth

References

Garside, J. and Larson, M. A., 1978, Direct Observations of Secondary Nuclei, *J. Cryst. Growth* **43**, 694.

Larson, M. A. White, E. T., Ramanarayanan, K. A., and Berglund, K. A., 1985, Growth Rate Dispersion in MSMPR Crystallizers, *AIChE J.* **31**(1), 90-94.

Ramanarayanan, K. A., 1982, Production and growth of contact nuclei. Ph.D. Dissertation, Iowa State University of Science and Technology, Ames, Iowa.

Randolph, A. D. and White, E. T., 1977, Modeling Size Dispersion in the Prediction of Crystal Size Distribution. *Chem. Eng. Sci.* **32**, 1067-1076.

Ristic, R.I., J. N. Sherwood, and T. S. Shripathi, 1991, The Role of Dislocations and Mechanical Deformation in Growth Rate Dispersion in Potash Alum Crystals, *Advances in Industrial Crystallization*, pp. 77-91. Butterworth-Heinemann, Oxford.

White, E. T. and Wright, P. G., 1971, Magnitude of Size Dispersion Effects in Crystallization. *CEP Symp. Ser.* **67**(110), 81-87.

Zacher, U. and Mersmann, A., 1995, The influence of internal crystal perfection on growth rate dispersion in a continuous suspension crystallizer. *J. Cryst. Growth* **147**, 172-180.

CHAPTER 3. USING DISLOCATIONS AND INTEGRAL STRAIN TO MODEL THE GROWTH RATES OF SECONDARY NUCLEI

A paper submitted for publication in *Chemical Engineering Science*

Christopher M. Jones and Maurice A. Larson

Abstract

It has been observed in single crystal growth batch experiments where the solution is stagnant that different materials and different crystals crystallize with varying growth rate profiles. Growth rate dispersion has been shown to be a function of the supersaturation conditions present during both nucleation and growth. The purpose of this paper is to interpret the growth rate profiles of sodium nitrate, potash alum, and potassium sulfate nuclei through the development of a new growth rate model.

Introduction

Work performed with large potash alum crystals has shown conclusively that growth rates of single crystals are functions of both dislocation density and lattice strain (Ristic *et al.* 1991). Continuous crystallizer experiments using potash alum have also shown that integral strain is a function of supersaturation, and crystals with large degrees of strain do not grow to be large crystals in mixed-suspension, mixed-product removal (MSMPR) crystallizers (Zacher and Mersmann, 1995). Experiments performed on sodium nitrate secondary nuclei demonstrated that strain was not a large factor in determining their growth rates (Ristic *et al.*,

1997). The application of tensile strain to large sodium nitrate crystals showed that increasing the applied strain measurably decreased their growth rates in a time dependent manner. In contrast, the application of tensile strain to large potash alum crystals resulted in a step change in the growth rate without any time dependence.

The difference between the effect strain has on sodium nitrate and on potash alum has been proposed to be due to the fact that potash alum is more brittle than sodium nitrate. Sodium nitrate is a very ductile substance deforming plastically under high levels of strain. These plastic deformations manifest themselves as new growth sources in a crystal; new growth sources allow for faster growth rates. Ristic *et al.* (1997) showed that sodium nitrate crystals strained to fracture had a higher growth rate following the fracture than they did prior to the application of tensile strain.

Growth rate dispersion in crystallizing systems can be a result of varying levels of strain and dislocation density between crystals. Van der Heijden and van der Eerden (1991) were able to fit with high correlation the data of Ristic *et al.* (1988) with a grain boundary model of strain. Dislocation density has also demonstrated itself to be a factor in determining crystal growth rates. Garside and Davey (1980) modified the BCF model with the parameter, ε, that quantifies the extent to which groups of dislocations enhance the growth rate of a crystal. Assuming that different crystals in a system can have different surface characteristics and therefore different values of ε, this variation would be sufficient to cause growth rate dispersion. Two theoretical models exist that have experimentally and theoretically shown to be possible mechanisms of GRD in crystal systems--strain and dislocations.

In order to make crystallization processes more efficient, it is necessary to understand the mechanics of crystal growth, especially information about crystallizer conditions that can increase or decrease a crystal's growth rate. Empirical equations can often fit growth rate data from single crystal, stirred batch, or MSMPR experiments, but they are not the same as fitting a model built from basic principles. A model that successfully fits experimental data allows focus on areas that can make crystallization more efficient and more predictable by giving a direction to future research.

The purpose of this paper is to determine a growth rate model that can be supported both theoretically and experimentally. The model must allow for a crystal's growth rate to be a function of strain and dislocations, while also accounting for growth rate dispersion. The prediction of how growth rate distributions vary as functions of supersaturation conditions must also be possible using the model. .

Material and Methods

Single crystal growth rate experiments were performed using the cell described by Jones and Larson (1999). Potash alum, potassium sulfate, and sodium nitrate were used in different trials. The basic set-up procedure was the same for all runs: solution for a given material was saturated by keeping excess crystal in solution at desired temperature for at least five days. A parent crystal was mounted on the steel rod of the growth cell with epoxy. Once the epoxy was dry the cell was preheated and the saturated solution was added to the cell. A glass plate was placed over the top of the cell to seal the growth chamber and to prevent evaporation of the solvent.

The cell was then mounted on an optical microscope and the cell temperature raised to assure that no nuclei were present; this was also verified by visually inspecting the glass surface through the microscope. The temperature of the cell was then reduced to attain the desired supersaturation conditions for nucleation. Contact nuclei were formed by sliding the parent crystal across the glass plate separating the chambers of the cell. Contact nuclei were then selected for observation.

For all three materials, secondary nuclei were subjected to multiple supersaturations within a single trial. The sizes at various times were recorded using either VHS tape or by taking photographs at selected time intervals with a 35 mm camera. Photographs were digitally scanned and subjected to image analysis. Images from the VHS tape recording were immediately digitized using the Image Pro® image analysis software, which could then be used by Image Pro® to measure the size of nuclei at selected times.

Results

Two plots of size as a function of time are shown for sodium nitrate, each at different conditions, in Figures 3.1 and 3.2. The growth rates of sodium nitrate nuclei are time dependent immediately following nucleation or following an increase in supersaturation. This is evident looking at Figure 3.1 where both events occur at different points during the run. Following nucleation and the step change increase in supersaturation, nuclei growth rates are initially at a high level and gradually decrease to a constant level after 3-5 minutes.

In Figure 3.2, crystals are nucleated and grown at the same supersaturation throughout the run. Immediately following nucleation, the growth rates of the nuclei are high. As the

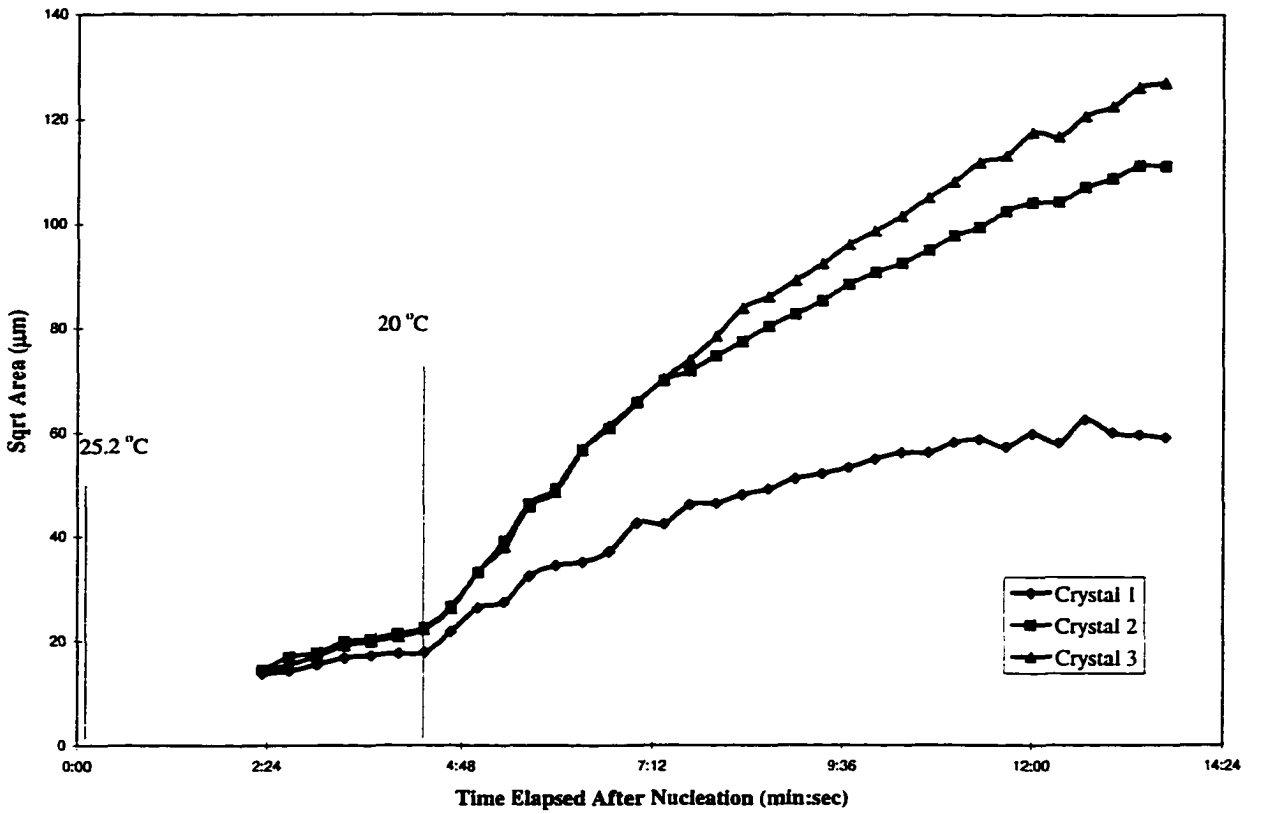

Figure 3.1 Growth history of three $NaNO_3$ crystals nucleated by contact from aqueous solution saturated at 27.45 °C

nuclei get larger, the crystal growth rates slow down, eventually reaching a near constant value after 3-5 minutes.

Both potash alum and potassium sulfate secondary nuclei exhibit nearly constant growth rates with respect to time. Only slight decreases can be seen in the growth rates of the potash alum crystals even over 15 minutes. Changing supersaturation resulted in step changes in the growth rate. Figure 3.3 records the sizes of potash alum secondary nuclei at selected times. Potash alum secondary nuclei were nucleated and grown at a given set of conditions; the supersaturation was changed at two different points during the growth period. The first change was an increase in supersaturation, and the second change was a decrease in the supersaturation. Figure 3.4 records the sizes of potassium sulfate secondary nuclei at various times. The potassium sulfate nuclei were nucleated and grown at a given supersaturation. Later in the run, the supersaturation was increased.

Discussion

Model

From the BCF model of crystal growth (Burton *et al.*, 1951) and Garside and Davey (1980), the growth rate can be modeled as

$$R = C\sigma_1\varepsilon\left(\frac{\sigma}{\sigma_1}\right)^2 \tanh\left(\frac{\sigma_1}{\varepsilon\sigma}\right) \tag{3.1}$$

The parameter, σ_1, is a function of the step height, the mean displacement of an adsorbed particle, the absolute temperature, and the edge energy of a nucleus per molecule. The parameter σ is the relative supersaturation present during growth. The lattice strain energy,

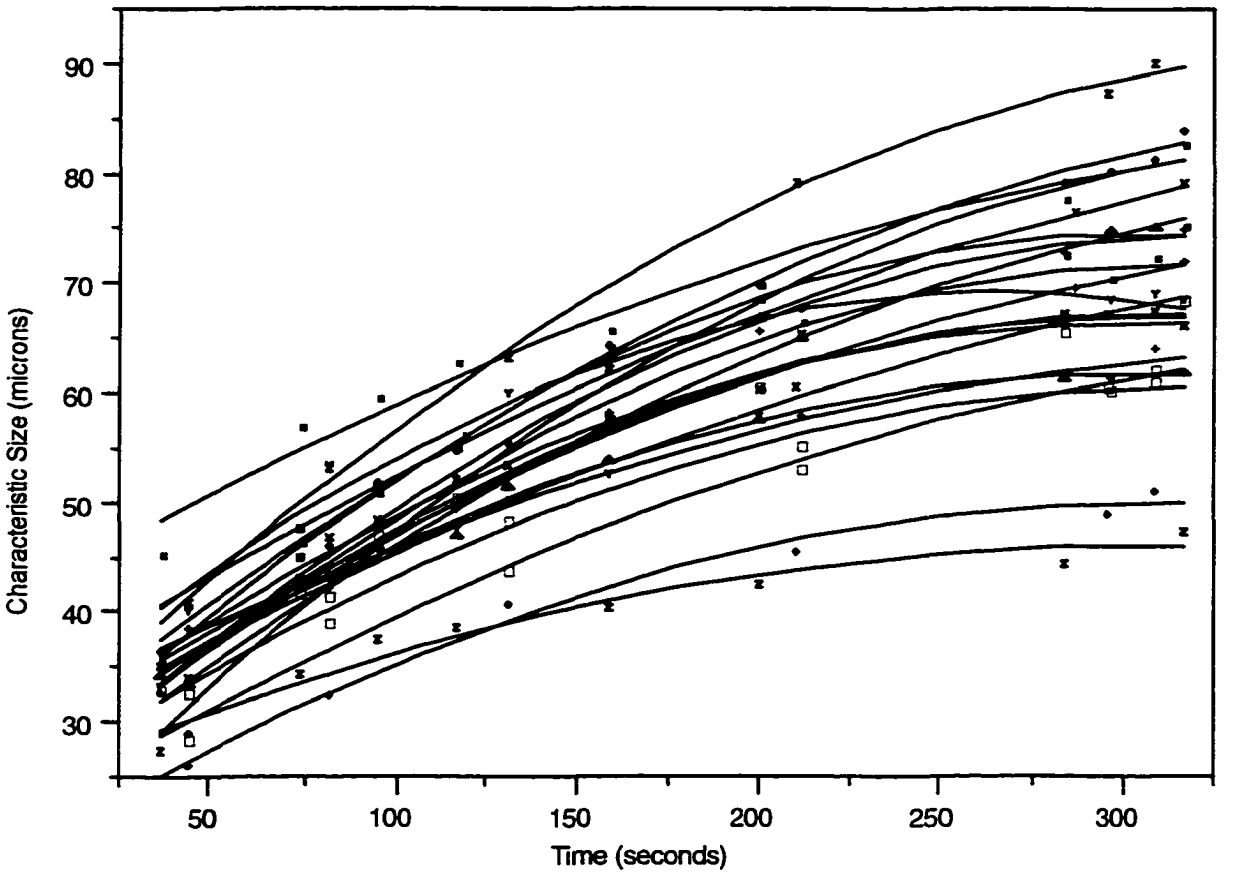

Figure 3.2 Length (μm) with respect to time (sec) of 21 $NaNO_3$ crystals saturated at 34.3 °C and nucleated and grown at 31°C

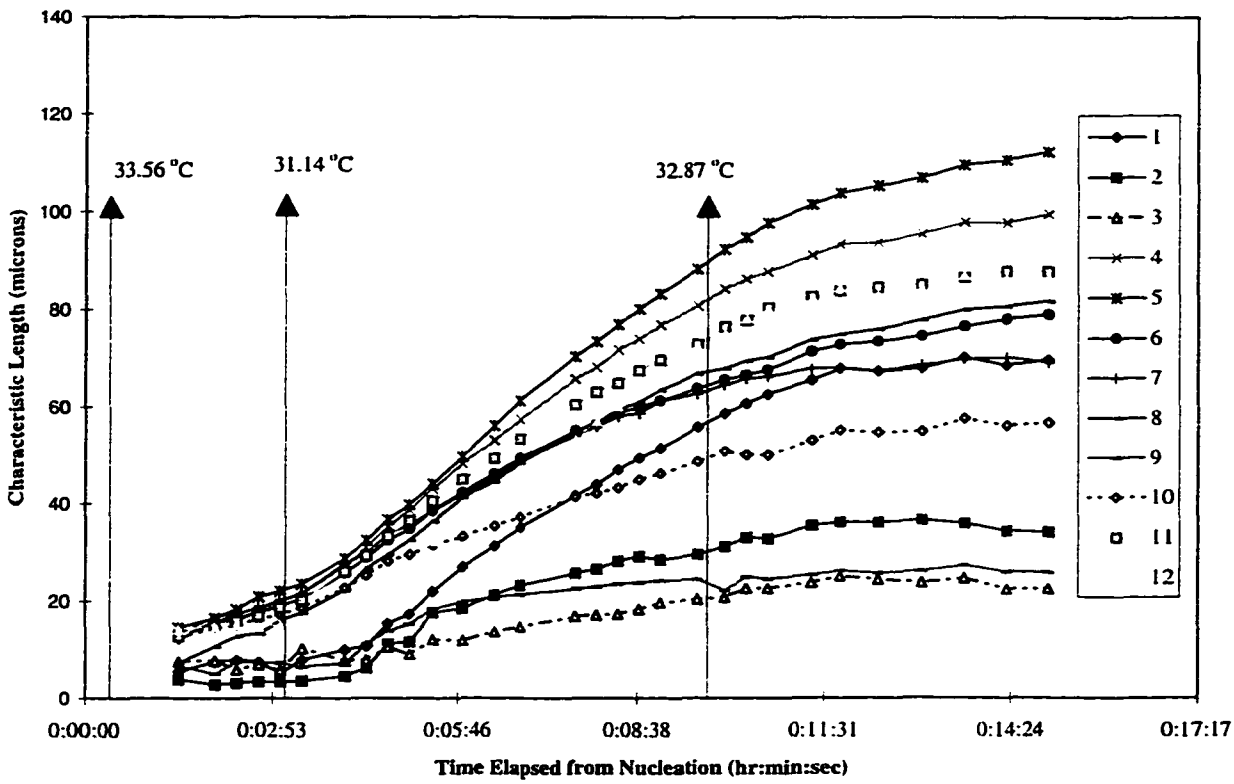

Figure 3.3 Growth history of twelve potash alum crystals nucleated by contact from aqueous solution saturated at 38.2 °C

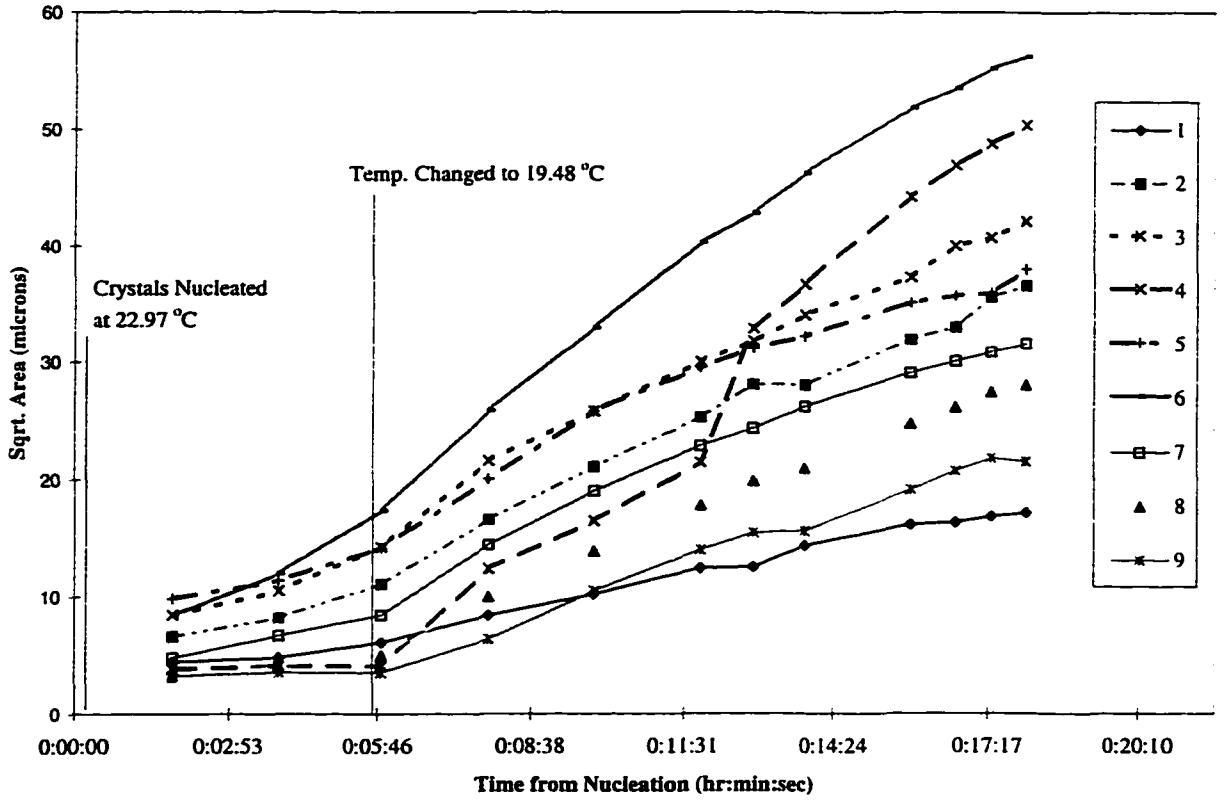

Figure 3.4 Size of nine potassium sulfate crystals as a function of time where solution was saturated at 26.6 °C

W, for a single particle using a grain boundary model was deduced by van der Heijden and van der Eerden (1991) and is defined as,

$$W(\eta, L) = \frac{3\mu b\Omega}{8\pi(1-\nu)\sqrt{l}} \frac{\eta}{\sqrt{L}} \ln\left(\frac{\alpha b}{4\pi r_c \sqrt{l}} \frac{\sqrt{L}}{\eta}\right) \tag{3.2}$$

The relative supersaturation, σ, is used to estimate the dimensionless driving force, $\frac{\Delta\mu}{kT}$, between the substance in the supersaturated solution and in the crystal. Having strain in the crystal adds to the chemical potential of the crystal. The driving force term, σ, can be corrected to deal with the effect of integral strain by subtracting W/kT from σ in Equation 3.1 which yields,

$$R = C\sigma_1 \varepsilon \left(\frac{\sigma - \frac{\frac{3\mu b\Omega}{8\pi(1-\nu)\sqrt{l}} \frac{\eta}{\sqrt{L}} \ln\left(\frac{\alpha b}{4\pi r_c \sqrt{l}} \frac{\sqrt{L}}{\eta}\right)}{kT}}{\sigma_1} \right)^2 \tanh\left(\frac{\sigma_1}{\varepsilon\left(\sigma - \frac{\frac{3\mu b\Omega}{8\pi(1-\nu)\sqrt{l}} \frac{\eta}{\sqrt{L}} \ln\left(\frac{\alpha b}{4\pi r_c \sqrt{l}} \frac{\sqrt{L}}{\eta}\right)}{kT} \right)} \right) \tag{3.3}$$

Equation 3.3 is a new growth rate model that incorporates integral strain into the driving force term of the dislocation controlled growth rate model. Equation 3.3 can be simplified further by defining a pseudo relative supersaturation, y,

$$y = \frac{\sigma - \dfrac{\dfrac{3\mu b\Omega}{8\pi(1-\nu)\sqrt{l}}\dfrac{\eta}{\sqrt{L}}\ln\left(\dfrac{\alpha b}{4\pi r_c\sqrt{l}}\dfrac{\sqrt{L}}{\eta}\right)}{kT}}{\sigma_1} \tag{3.4}$$

Inserting y into Equation 3.3 yields a simplified growth rate expression,

$$R = C\sigma_1\varepsilon(y)^2\tanh\left(\frac{1}{\varepsilon y}\right) \tag{3.5}$$

The dimensionless growth rate, $\frac{R}{C\sigma_1}$, is plotted as a function of ε for various values of y in Figure 3.5. Figure 3.5 shows that for a fixed value of ε, that the growth rate will increase with increasing values of y. The dimensionless growth rate will also increase with increasing values of ε at fixed values of y.

The range of possible values for the dimensionless growth rate increases with increasing y. A range of values can be calculated for a given value of y because increasing ε values past 8 does not have an appreciable effect on the dimensionless growth rate. $\frac{R}{C\sigma_1}$ reaches an asymptotic value as ε gets large. In Figure 3.6 the range of possible values of $\frac{R}{C\sigma_1}$ are plotted with respect to the pseudo relative supersaturation, y. While the specific spread of growth rates for any system of crystals will depend in part upon the distribution of ε values in the system, the spread of the distribution will be limited by the distribution of y values in the system. Figure 3.6 demonstrates that increasing values of y will allow for increasing variability in the growth rate distribution.

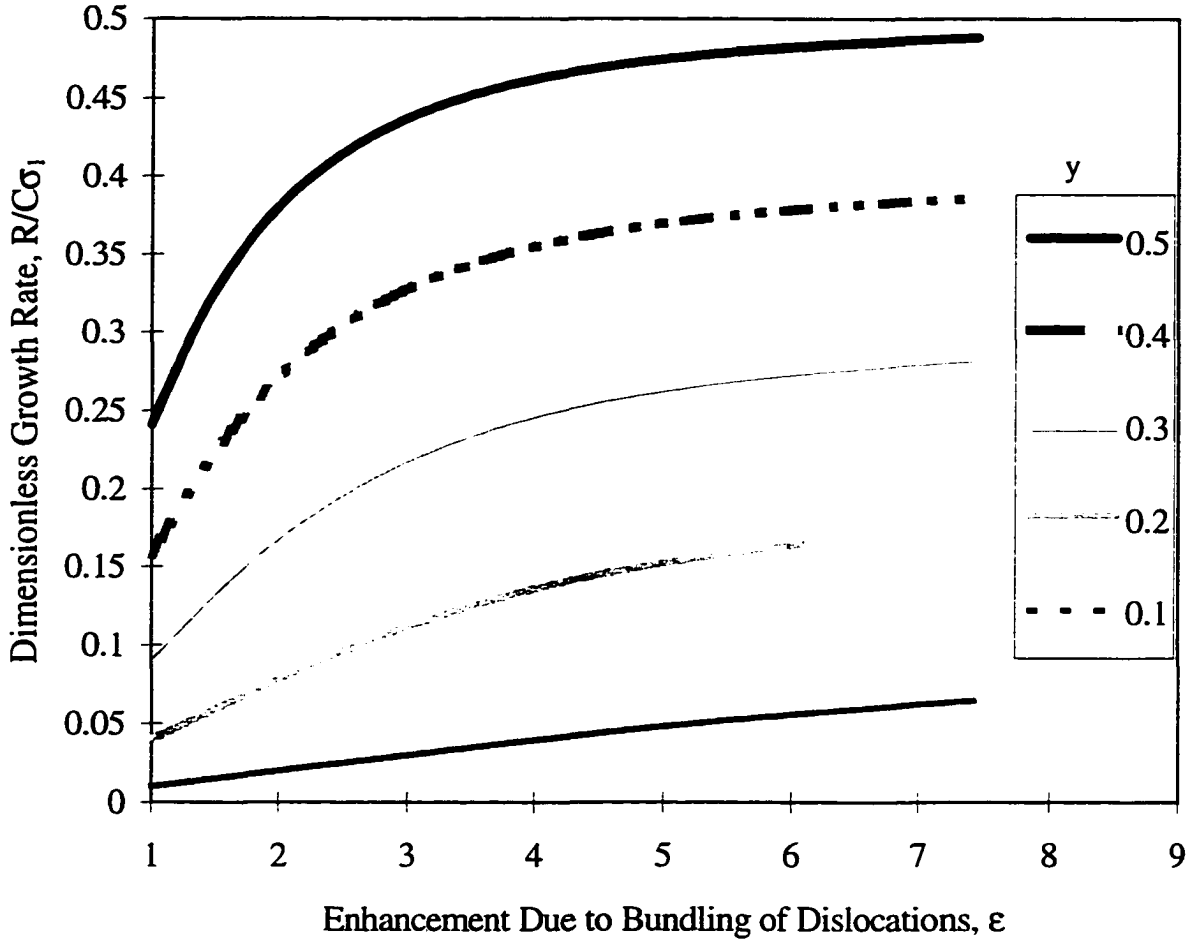

Figure 3.5 Plot of $R/C\sigma_1$ as a function of ε for various levels of y

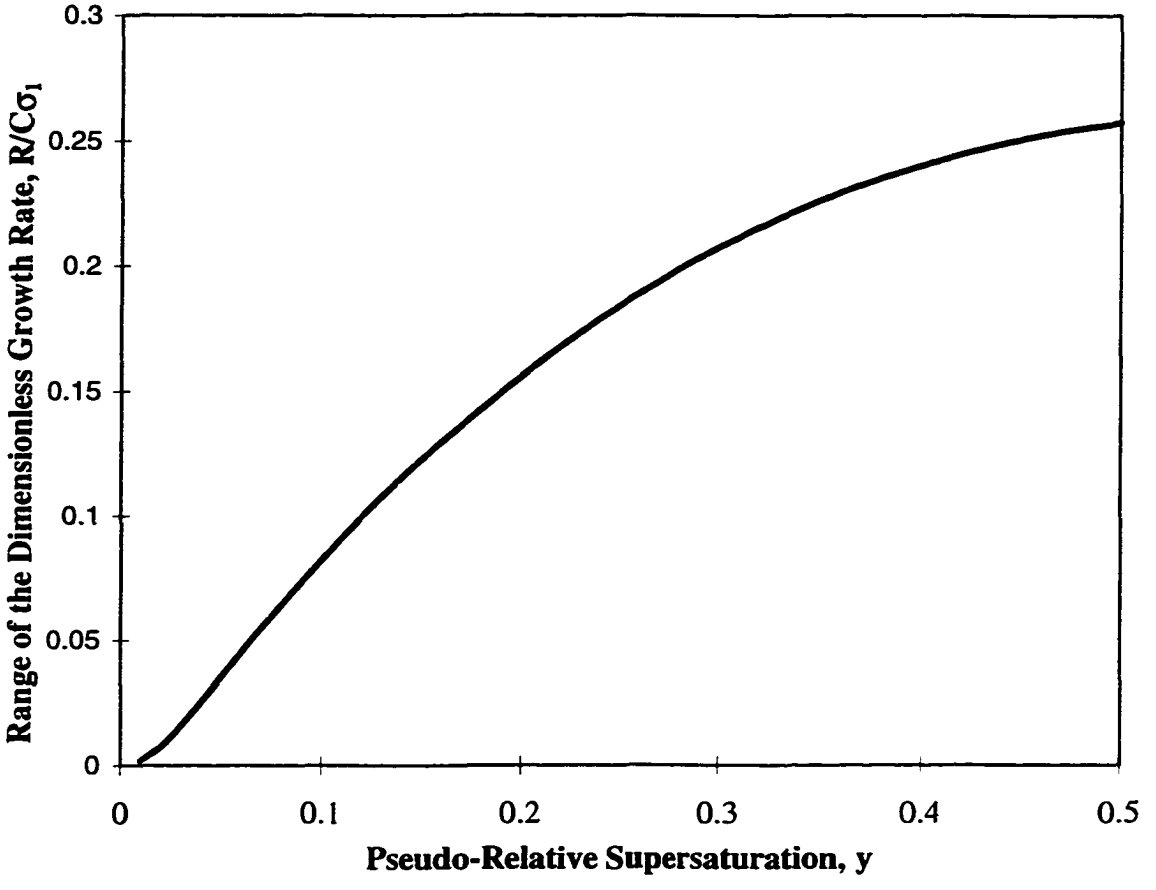

Figure 3.6 The range of the dimensionless growth rate is plotted as a function of y

Lattice Strain Energy. Both the mean and spread of the distribution of R are highly dependent upon the value of y. Because σ is known for a system, characterizing the response of y requires an analysis of how the lattice strain energy, W, varies with changing system parameters. Rearranging Equation 3.2,

$$\frac{8\pi(1-\nu)\sqrt{l}}{3\mu b\Omega}W = \frac{\eta}{\sqrt{L}}\left(\ln\left(\frac{\alpha b}{4\pi r_c\sqrt{l}}\right)+\ln\left(\frac{\sqrt{L}}{\eta}\right)\right) \tag{3.6}$$

defining x, A, and z as,

$$x = \frac{8\pi(1-\nu)\sqrt{l}}{3\mu b\Omega}W \tag{3.7}$$

$$A = \ln\left(\frac{\alpha b}{4\pi r_c\sqrt{l}}\right) \tag{3.8}$$

$$z = \frac{\sqrt{L}}{\eta} \tag{3.9}$$

yields the expression,

$$x = \frac{1}{z}(A+\ln(z)) \tag{3.10}$$

In Equation 3.10, x represents a reduced form of W. W increases with increasing x, and W decreases with decreasing x. The independent variable, z, can be changed by altering L or η. This implies a degree of size dependency in the grain boundary strain model. In Figure 3.7, x is plotted as a function of z for various values of the parameter A. At appropriate levels of A increasing η or decreasing L will increase W, decrease y, and decrease the value of R. Ristic *et al.* (1991) showed that increasing integral strain decreased crystal growth rates. This means that A must be greater than approximately 1, otherwise, W will

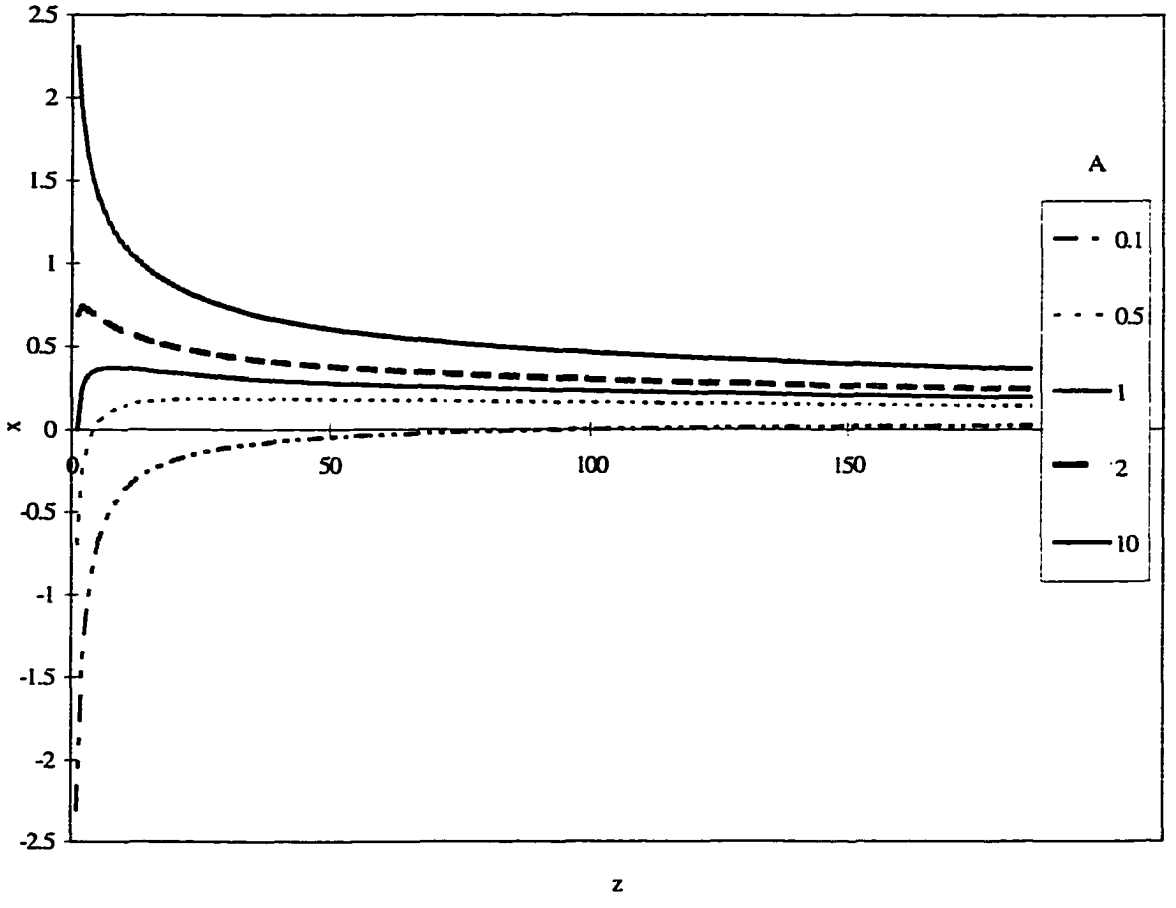

Figure 3.7 Plot of the reduced lattice strain energy x as a function of z for various values of A

decrease with increasing strain, and that would be contrary to what has been reported experimentally. A is a function of the grain boundary size l, the burgers vector b, the parameter α which is a function of the Poisson ratio. The parameter α is defined as

$$\alpha = \exp\left(\frac{3}{4(1-\nu)}\right) \tag{3.11}$$

and the critical defect radius, r_c. These parameters are expected to vary from substance to substance. Changes in these parameters alter the operating curve in Figure 3.7, and as a result, the effect strain will have on a crystal's growth rate.

Comparing Model Parameters with Experimental Results

Time Dependent Manifestation of Strain. Different substances exhibit different growth rate profiles in single growth experiments. Potash alum, in Figure 3.3, has an almost constant growth rate for any given supersaturation with only a very small decrease after 20 minutes in the cell. Potassium sulfate, in Figure 3.4, has a similar growth rate profile. In contrast, sodium nitrate, in Figures 3.1 and 3.2, exhibits a decreasing growth rate immediately following nucleation. Following a step change increase in supersaturation, the growth rate will increase initially and then decrease to a constant level. The model in Equation 3.4 predicts the growth rate will decrease if the supersaturation decreases or if the strain increases. Because the reduction in growth rate for the sodium nitrate crystals does not correspond with the reduction in growth rate seen for potash alum or potassium sulfate, it can be inferred that sodium nitrate nuclei growth rates decrease for a reason other than decreasing supersaturation.

Remembering that the results of Ristic *et al.* (1997) show that large sodium nitrate crystals subjected to tensile strain had time dependent growth rate behavior points to a possible explanation. Sodium nitrate is ductile, and as a result, it plastically deforms over time producing dislocations in the process. Eventually a strained crystal will reach strain-lattice equilibrium, and the growth rate will reach a constant value. Regardless of the source of strain, a sodium nitrate crystal subjected to a step change in strain can be expected to behave in a similar manner.

In experiments by Jones and Larson (1999), thousands of sodium nitrate secondary nuclei were formed and their growth rate profiles were recorded. Figure 3.8 shows the relationship between the initial growth rate and the value of the growth rate deceleration for crystals used in set #1 of Jones and Larson (1999). Figure 3.9 shows the same relationship using the data from set #2 of Jones and Larson (1999). Even though crystals were nucleated and grown under different conditions in Figures 3.8 and 3.9, there is a strong correlation between the initial growth rate and the level of growth rate deceleration for all crystals.

Higher initial growth rates correspond with higher levels of growth rate deceleration. *A* linear deceleration of the growth rate with respect to time corresponds with the observed relaxation phenomenon for an applied tensile stress in sodium nitrate crystals as reported by Ristic *et al.* (1997). If a stress is applied suddenly to a sodium nitrate crystal, it is proposed that the integral strain of the crystal increases in a time dependent manner. Immediately following application of the strain the growth rate was a linear function with respect to time (Ristic *et al.* 1997).. Sodium nitrate contact nuclei demonstrate a similar dependence upon time, as in Equation 3.12,

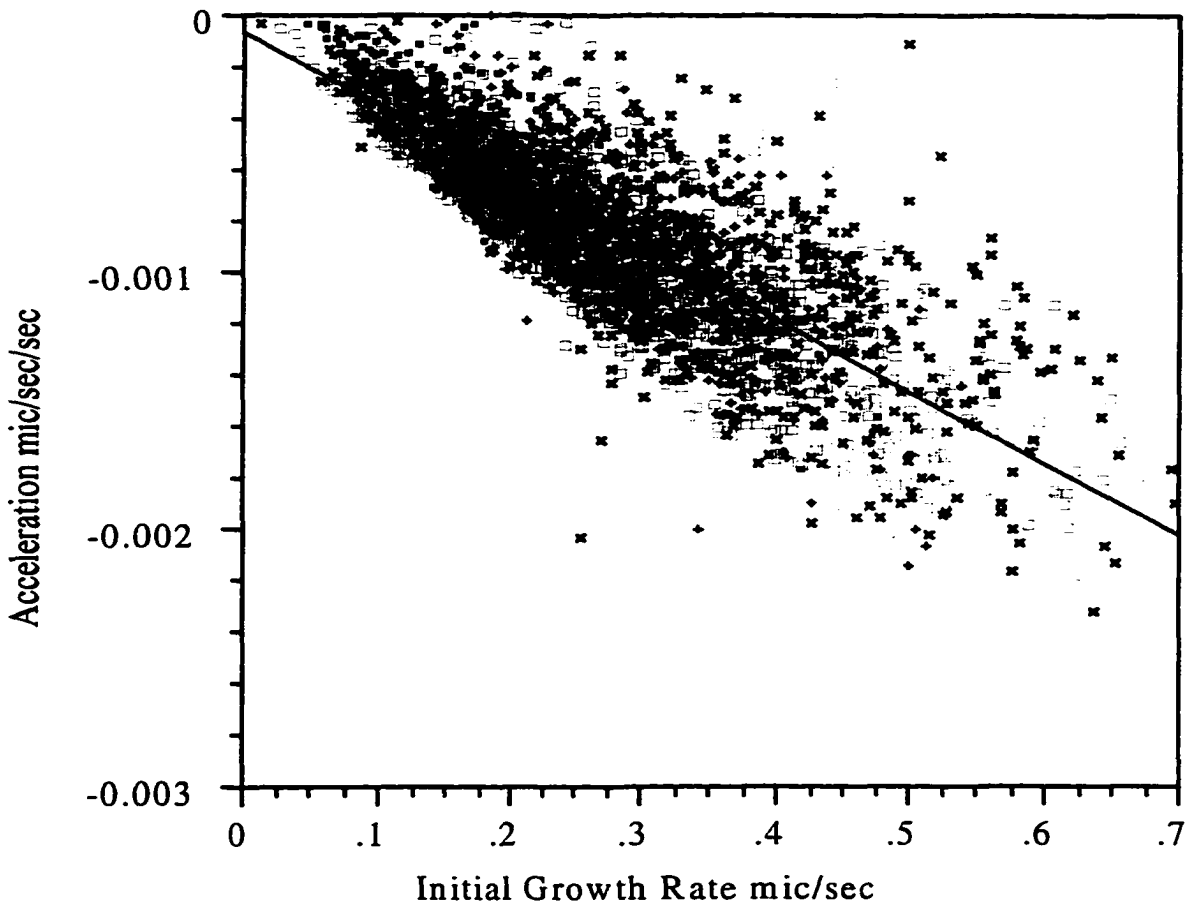

Figure 3.8 Plot of the deceleration of a sodium nitrate crystal's growth rate as a function of the initial growth rate for all crystals in set #1 of Jones and Larson (1999); symbols refer to the supersaturation conditions for that crystal

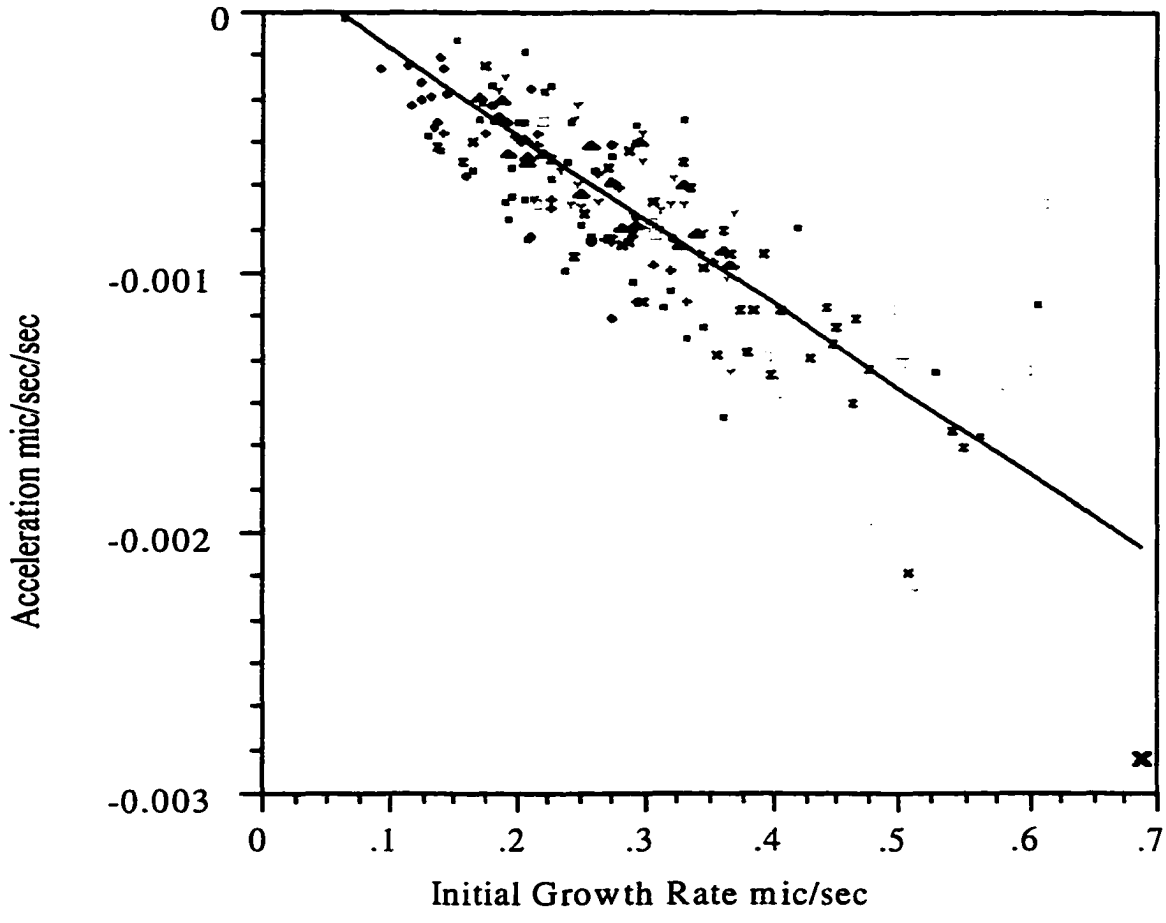

Figure 3.9 Deceleration of a sodium nitrate crystal's growth rate as a function of the initial growth rate for all crystals in set #2 of Jones and Larson (1999); symbols refer to the supersaturation conditions for that crystal

$$R = 2a_r t + b_r \tag{3.12}$$

and it is reasonable to assume that the cause is also due to strain. Nuclei that are growing rapidly at nucleation are most likely the nuclei with the highest level of defects. Step increases in supersaturation can also be a source of defects. As the lattice approaches equilibrium with the level of strain caused by those defects, the growth rate of the crystal slows eventually reaching a constant value. In Figure 3.7 this would be equivalent to x decreasing as time progressed.

Potash alum and potassium sulfate do not exhibit this time dependent growth rate behavior. Following nucleation or any step change in the supersaturation is a corresponding step change of the growth rate. The main difference between potash alum and sodium nitrate is their ductility. Brittle substances like potash alum and potassium sulfate will not exhibit time dependent growth rates for constant supersaturations on the time scale usually observed in a crystallizer.

Ristic *et al.* (1997) demonstrated that the level of growth rate deceleration increased with the degree of the step change in applied strain for sodium nitrate crystals. Large increases of applied tensile strain resulted in large values of growth rate deceleration, while small increases yielded small values of the deceleration. Immediately following application of the strain the growth rate varied with time in a linear fashion. It is inferred that the nucleation event is a source of strain in nuclei, where faster growing sodium nitrate crystals also have the largest levels of strain. Nuclei, whether they are formed by primary or secondary nucleation, are formed very quickly. The speed with which this process takes place also determines the initial levels of strain a crystal will have.

Interpreting GRD Results as a Function of ε and η. Jones and Larson (1999) report that the mean of the initial growth rate distribution can be manipulated by changing both the nucleation and growing supersaturations, while the standard deviation was shown only to be a function of the growing supersaturation. This does not mean the standard deviation of the initial growth rate distribution is not a function of the nucleation supersaturation, rather it means that the statistical tests did not prove the effect due to nucleation supersaturation to be statistically significant. The distribution of R for any given set of conditions can be assumed to be a gamma distribution. Both ε and y can be and probably are functions of both the nucleation and growing supersaturations. For any given system of crystals there will be a distribution of ε, η, and y. Determining these distributions is mathematically difficult, so a more qualitative approach is preferred.

The pseudo relative supersaturation, y, is a function of σ and of η, where σ is the growing supersaturation and η is the integral strain of the crystals. The integral strain, η, is most likely a function of the nucleation supersaturation, where higher nucleation supersaturations cause higher levels of strain. By this reasoning, R can be increased by increasing the growing supersaturation and by decreasing the nucleation supersaturation. The response surface of the mean of the initial growth rate distribution is a function of the nucleation and growing supersaturations (Jones and Larson, 1999). This trend is observed only in the portion of the surface where the growing relative supersaturation is greater than 0.04. At values less than 0.04, increasing the nucleation relative supersaturation increases the mean of the initial growth rate distribution.

For a given system of crystals there is a distribution of ε. The mean value of ε is most likely increasing with increasing nucleation supersaturation, where the enhancement due to bundling of dislocations increases with increasing dislocation density. A point is reached where increases in the initial growth rate due to increasing ε are counteracted by the effect of increasing η on y. For sodium nitrate that point has been determined experimentally to be where the growing relative supersaturation is 0.04. Crystals at the same growing supersaturation, greater than 0.04 for sodium nitrate, will, on average, grow faster with fewer defects and less strain. At low levels of the growing supersaturation, less than 0.04 for sodium nitrate, crystals will, on average, grow faster with more growth sources. It is unknown whether substances other than sodium nitrate would exhibit the same behavior due to the differences in ductility, but it is not out of the question. It is more likely that there will be a transition point from dislocation control to strain control that will vary from material to material.

The behavior of standard deviation of the initial growth rate distribution is a function only of the growing supersaturation (Jones and Larson, 1999). The plot in Figure 3.6 points to the explanation. High levels of the growing supersaturation correspond with higher levels of y. An increase in y will assure that the distribution of R always increases. Low levels of y will always give low standard deviations of the initial growth rate distribution because the range of the possible growth rates is smaller at low y than it is at high y. For sodium nitrate, high levels of integral strain are needed to affect secondary nuclei initial growth rates because of the time dependent behavior of strain in ductile materials. While the standard deviation of a growth rate distribution would be a function of the nucleation supersaturation, it would not

be a strong function relative to the growing supersaturation. This explains why the standard deviation does not show up as a statistically significant function of the nucleation supersaturation.

Conclusions

The time dependent behavior of the growth rate of sodium nitrate secondary nuclei is most likely due to the time dependence of sodium nitrate's growth rate to an initial level of strain. Brittle substances like potash alum and potassium sulfate do not exhibit time dependent growth rates following nucleation. The ductility of the crystallizing material plays an important role in determining the growth rate profile of a crystal.

The model in Equation 3.3 allows for a crystal's growth rate to be dependent upon both dislocation density and strain. The parameter ε will increase with increasing dislocation density. These factors increase with increasing nucleation supersaturation. However, it is known from experiments that increasing ε has an opposite effect than increasing η on the growth rate of a crystal. From Jones and Larson (1999) it is suspected that ε is growth rate controlling at low levels of growing supersaturation, while integral strain is growth rate controlling at high levels of growing supersaturation.

Equation 3.3 is also consistent with the result of Jones and Larson (1999). They demonstrated that increasing growing supersaturation results in an increase in the spread of the growth rate distribution. Equation 3.3 allows for the effect of the nucleation supersaturation on the spread of the initial growth rate distribution; this would be a result of how ε and η are distributed for a given set of conditions. However, the relationship of the

spread to the growing superaturation is an effect of greater magnitude, and will show up more readily in experiments.

Acknowledgments

The authors would like to thank Wayne Genck of Genck International for his financial support of this research project.

Nomenclature

b	Burgers vector (microns)
t	Time (seconds)
r_c	Critical radius of defect (microns)
L	Crystal size (microns)
l	Average length of mosaic block (microns)
a_r, b_r	Growth rate constants
C	BCF model constant (microns/sec)
R	Crystal growth rate (microns/sec)
k	Boltzmann's constant (Joules/K)
T	Absolute temperature (K)
W	Lattice strain energy (Joules)

Greek Symbols

ε	Enhancement factor due to bundling of dislocations
η	Integral strain (degrees)
μ	Shear modulus (newtons/microns^2)
ν	Poisson's ratio

σ Relative supersaturation

σ_1 BCF model constant

Ω Molecular volume (microns^3)

References

Burton, W. K., N. Cabrera, and F. C. Frank, 1951, The Growth of Crystals and the Equilibrium Structure of their Surfaces, *Phil. Trans. Roy. Soc.* **243**, 299-358.

Jones C. M., and Larson, M. A., Characterizing Growth Rate Dispersion of $NaNO_3$ Secondary Nuclei as a Function of Supersaturation, paper submitted to *AIChE J.* January 1999.

Garside, J. and Davey, R. J., 1980, Secondary Contact Nucleation: Kinetics, Growth and Scale-Up, *Chem. Eng. Commun.* **4**, 393-424.

Ristic, R.I., J. N. Sherwood, and T. S. Shripathi, 1991, The Role of Dislocations and Mechanical Deformation in Growth Rate Dispersion in Potash Alum Crystals, *Advances in Industrial Crystallization*, pp. 77-91. Butterworth-Heinemann, Oxford.

Ristic, R.I., J. N. Sherwood, and T. S. Shripathi, 1997, The influence of tensile strain on the growth rates of potash alum and sodium nitrate, *J. Cryst. Growth* **179**, 194-204.

Ristic, R. I., J. N. Sherwood, K. Wojciechowsky, 1988, Assessment of the Strain in Small Sodium Chlorate Crystals and its Relation to Growth Rate Dispersion, *J. Cryst. Growth* **91**, 163-168.

van der Heijden, A. E. D. M. and van der Eerden, J. P., 1992, Growth rate dispersion: the role of lattice strain, *J. Cryst. Growth* **118**, 14-26.

CHAPTER 4. THE ROLE OF DISLOCATIONS, INTEGRAL STRAIN, AND SUPERSATURATION ON THE GROWTH RATES OF SODIUM NITRATE

A paper to be submitted for publication in *Journal of Crystal Growth*

Christopher M. Jones, Maurice A. Larson, Radoljub I. Ristic, and John N. Sherwood

Abstract

Integral strain and dislocations have both been cited as determining factors of crystal growth rates. Sodium nitrate growth rate distributions have shown dependence upon the supersaturation present during nucleation and during growth. This paper provides further evidence that crystal growth rates are dependent upon both dislocations and strain. It also demonstrates the mechanism of crystal growth at low supersaturation levels and the difference in the dependence of crystal growth rates with respect to integral strain at varying supersaturations.

Introduction

Ristic *et al.* (1991) demonstrated that strain has an effect on the growth rates of a variety of materials crystallizing from solution. Increasing the level of integral strain in a crystal decreased the growth rate of macro sized potash alum, sodium chlorate, and sodium nitrate crystals. Ristic *et al.* (1997) have also shown that secondary nuclei react to various levels of strain differently, depending upon the physical properties of the crystal whose growth behavior is being studied. Brittle materials have a step change response of the growth

rate after the application of tensile strain. Sodium nitrate, which is ductile had a time dependent decrease in the growth rate after the application of tensile strain.

The growth rates of potash alum and sodium chlorate nuclei were both shown to be inversely proportional to the level of integral strain (Ristic *et al.*, 1988 and Ristic *et al.*, 1991). Experiments with sodium nitrate nuclei demonstrated a limited effect on the growth rate due to variations of integral strain from crystal to crystal at similar levels of relative supersaturation (Ristic *et al.*, 1997) For all three materials the relative supersaturation was at about 0.35% using g/g sol for units of concentration.

The purpose of this paper is to investigate the effect of strain on sodium nitrate secondary nuclei as a function of supersaturation. Furthermore, comparisons of results will be made to the strain-dislocation model proposed by Jones and Larson (1999b).

Materials and Methods

Nuclei

Sodium nitrate crystals were nucleated by contact in the batch cell described in Jones and Larson (1999a) and subjected to a given set of supersaturation conditions. Solution was saturated at 34.3 °C. Crystals were nucleated at 31 °C, and the supersaturation was changed during the growth period by changing the temperature to 27 °C after approximately five minutes of growth. This corresponds to relative supersaturations of 1.51% at nucleation and 3.4% during the second growth period. Relative supersaturations were calculated using units of g/g solution for concentration. Crystals growth rates were determined by taking photographs of nuclei at selected intervals of time with a 35mm camera. The photographs

were digitally scanned and subjected to image analysis using Image Pro. Crystals sizes were plotted as a function of time and crystal growth rates were determined.

Once the nuclei had reached the size of 150 microns, nuclei were removed for Laue diffraction and subsequent integral strain analysis. Usually only one or two crystals could be removed from any single experiment. Crystals were sent to Dr. Sherwood's research group at the University of Strathclyde in Scotland, where Synchrotron radiation was used as the X-ray source to perform Laue diffraction. The integral strain was determined using the method described by Ristic *et al.* (1988). The defining equation is in Equation 4.1, where R is the radial asterism of a Laue spot, d is the specimen to film distance, θ is the reflection angle, and η is the integral strain. Several reflections measured at different radii were measured and averaged to derive the integral strain.

$$R = \frac{2\eta d}{\cos^2(2\theta)} \tag{4.1}$$

In separate experiments high resolution powder diffraction was used to determine if crystals of different sizes could be differentiated for differing levels of strain by variations in their powder diffraction spectra. The radiation used was a MoKα=0.701nm. This technique provided inconclusive results.

Macro Size Crystals

A macro sized sodium nitrate crystal was subjected to a flow of supersaturated solution in a growth cell, while also being subjected to laser interferometry. A schematic of the setup is displayed in Figure 4.1. Laser interferometry allows for the determination of the normal growth rate of a face *in situ* while also identifying growth sources on the face. The

supersaturation in the cell was changed by changing the flow of supersaturated solution to the cell. These experiments were performed at Strathclyde.

The normal growth rate, G, is determined using Equation 4.2 knowing the effective rate of steps, v, and the slope of the vicinal hillock, p,

$$G = pv \tag{4.2}$$

After determining the growth rates of the crystal at varying supersaturations, the crystal was removed, cleaved, and an X-ray surface topograph was taken to look for dislocations and regions of high strain in the crystal. X-ray surface topography allows characterizing the dislocation structure of the crystal.

Results and Discussion

Integral Strain of $NaNO_3$ Nuclei

The growth rates of 5 crystals, calculated during the second growth period where the relative supersaturation was 3.4%, are plotted with respect to the level of integral strain calculated using Laue diffraction in Figure 4.2.

The new data points are marked with squares, and they are fit with a solid line. The relative supersaturation was 3.4% for this data set. The dotted line represents the fitted relationship between strain and growth rate where the supersaturation was 0.32%. The data for the low level of supersaturation are taken from Ristic *et al.* (1997) and are represented by diamonds.

The effect of strain is more obvious and pronounced at high levels of growing supersaturation than it is at low levels. This correlates well with the reasoning of Jones and Larson (1999a) that the mean of the initial growth rate distribution of sodium nitrate

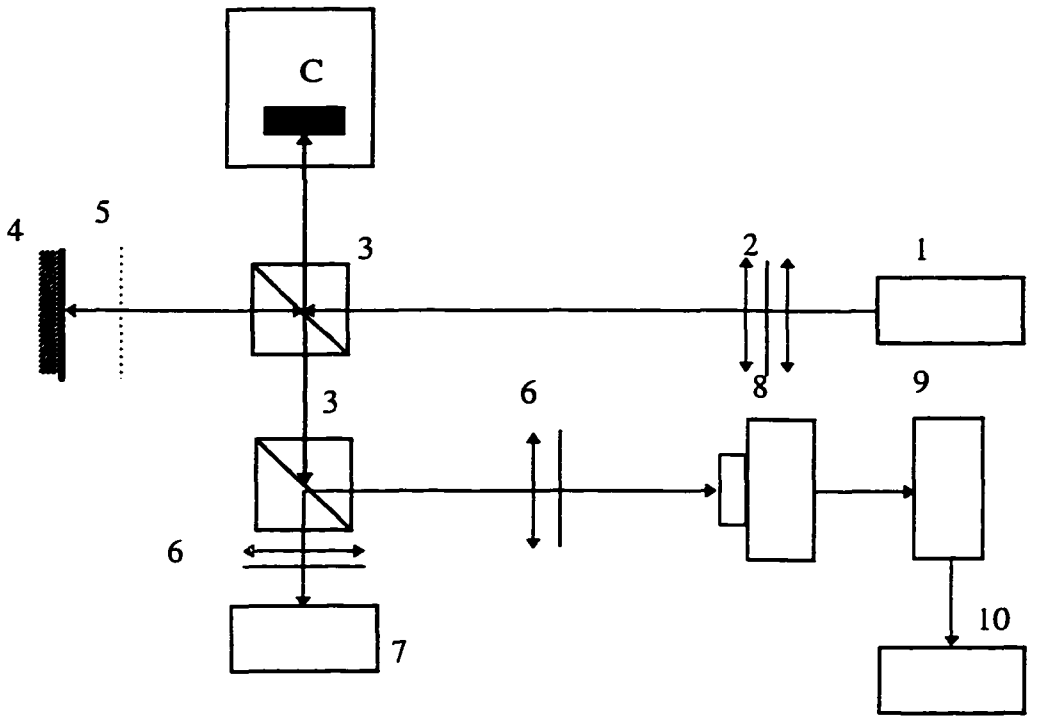

Figure 4.1 Optical scheme of the laser interferometry for *in situ* investigation of crystal growth from low temperature solutions of sodium nitrate: (1)lasers, (2)spatial filters and beam expanders, (3)beam splitters, (4)mirror, (5)neutral density filter, (6)objectives, (7)35mm cameras, (8 to 10) TV camera, monitor and chart recorder, (C)crystallization cell

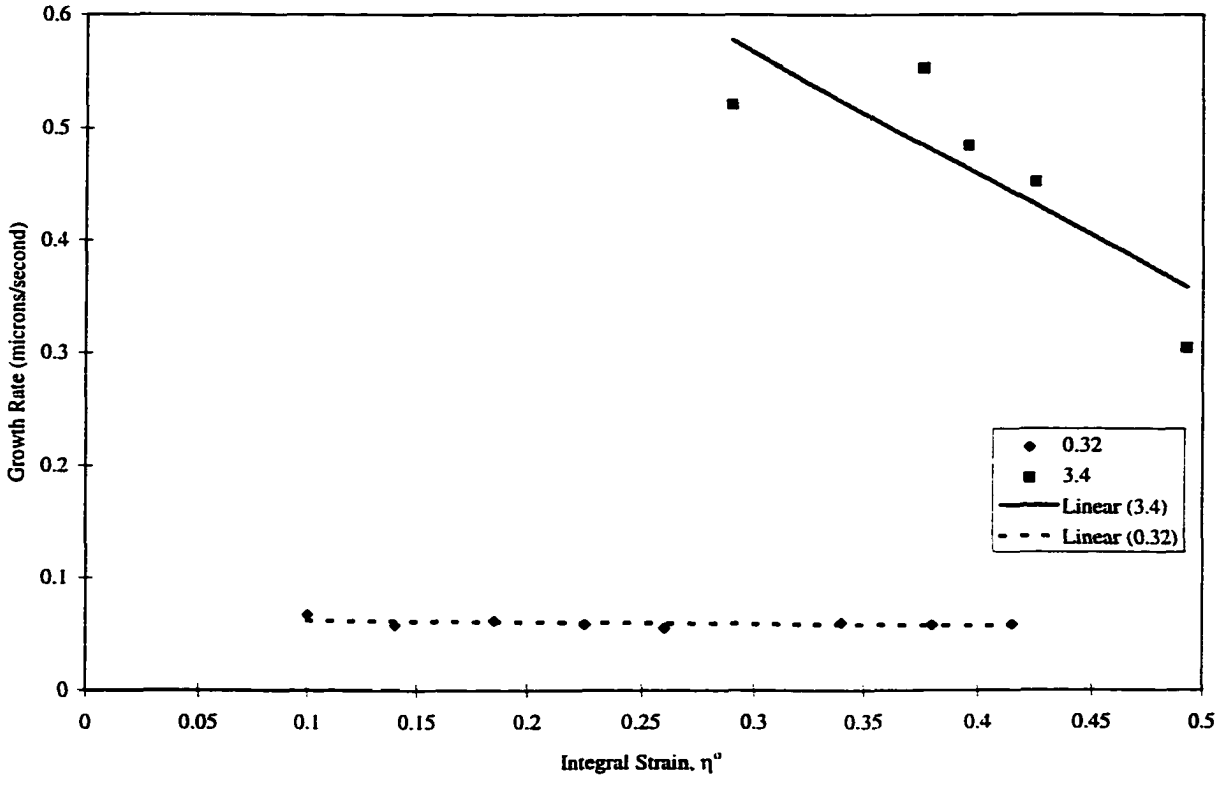

Figure 4.2 The growth rates of secondary sodium nitrate nuclei are plotted as a function of integral strain for two different supersaturations

secondary nuclei was strain controlled at higher levels of growing supersaturation. Unfortunately, the crystals were too small to perform X-ray surface topography, as that would have provided direct information about the dislocation structure of the nuclei.

Characterizing the Growth Rates of Macro Sized $NaNO_3$ Crystals

A large sodium nitrate crystal was grown in a cell that allowed for laser interferometry to be performed *in situ*. Figure 4.3 shows the laser interferogram of the [001] face of the sodium nitrate crystal studied in this experiment.

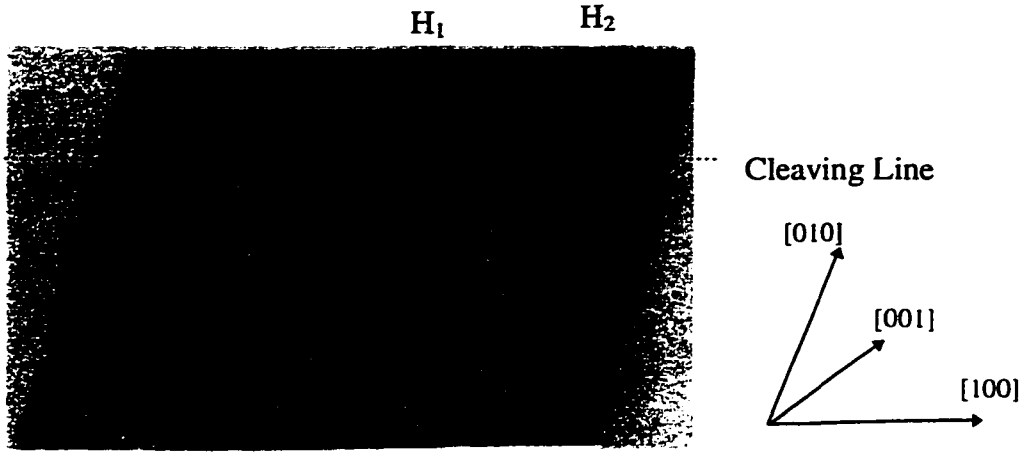

Figure 4.3 Laser interferogram of a macro sized sodium nitrate crystal

There are two growth sources shown in Figure 4.3, hillocks H_1 and H_2. The concentric rings surrounding these hillocks make them easy to identify. Figure 4.3 also shows the miller indices for the sodium nitrate crystal using a rhombohedral system. The indices are displayed at the right of the laser interferogram.

Figure 4.4 shows the fit of the growth rates of sodium nitrate derived using the laser interferometry technique with the BCF (Burton, *et al.*, 1951) dislocation controlled model.

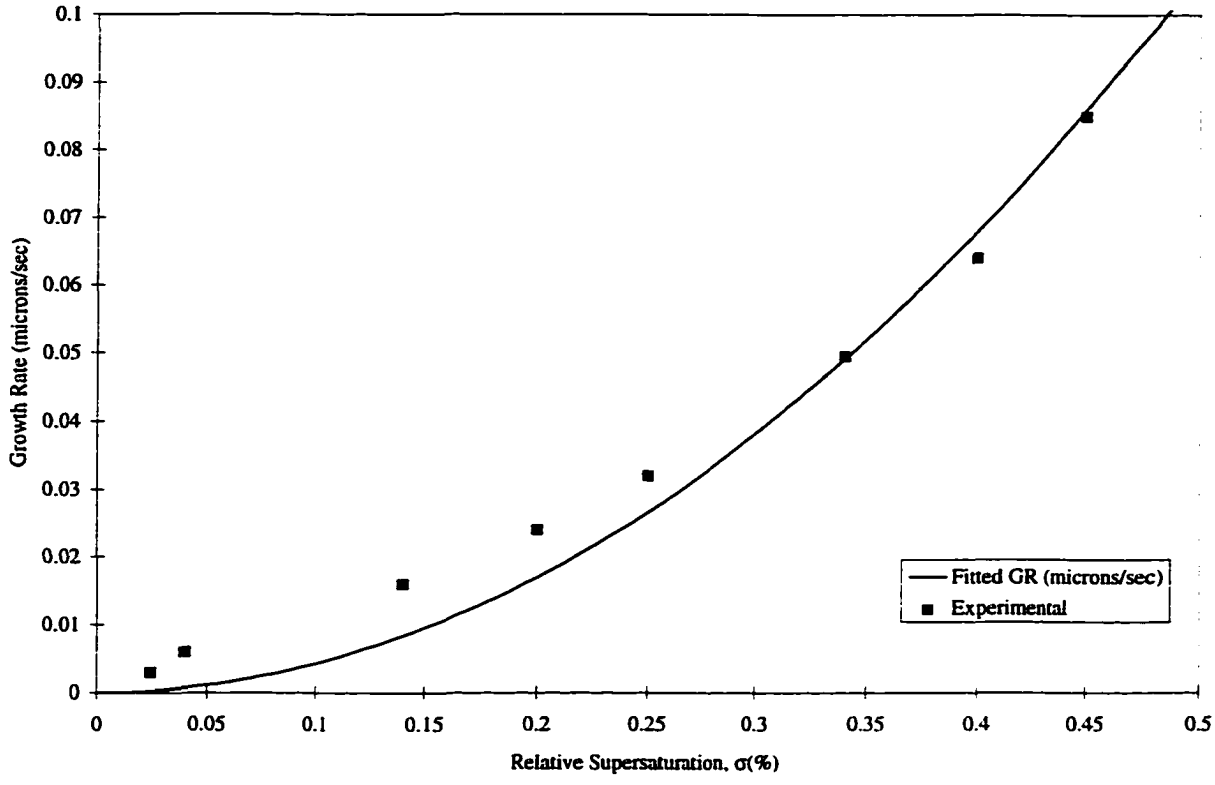

Figure 4.4 The normal growth rate of the [001] sodium nitrate face determined using laser interferometry and fit with the BCF growth model

There is good correlation between the predicted values and the experimental points. From these results, it is inferred that dislocation growth mechanism operates within the relative supersaturation region of $0.045<\sigma<0.45\%$. Increasing the relative supersaturation past 0.45% caused massive nucleation to occur such that the hillocks were no longer visible. Therefore, it was not possible to know for certain the growth rate mechanism at high supersaturation levels. At $\sigma<0.02\%$ the growth rate was extremely low and growth hillocks were not observable using laser interferometry. It is suspected that a 2-D nucleation growth mechanism was taking place under these conditions.

The secondary $NaNO_3$ nuclei used in the integral strain study by Ristic *et al.* (1997) were grown at supersaturations within the range. The new data was taken at a relative supersaturation of 3.4%. This was much higher than 0.45%. As a result it is not possible to know the mechanism of growth at those high levels of supersaturation for certain. It can be assumed that the growth hillocks would remain growth rate controlling until the supersaturation reached a point where the level of strain became rate controlling. The only other limit for growth rates known besides strain and dislocations are limits due to mass transfer, and mass transfer is not likely to be growth rate limiting for these supersaturations.

After kinetic measurements were finished with the macro sodium nitrate crystal, the crystal was cleaved and an X-ray topograph of the crystal was taken. The crystal was cleaved along the line indicated in Figure 4.3, and the top portion containing the two growth hillocks was subjected to surface topography. Figure 4.5 shows the surface topograph looking in the [010] direction.

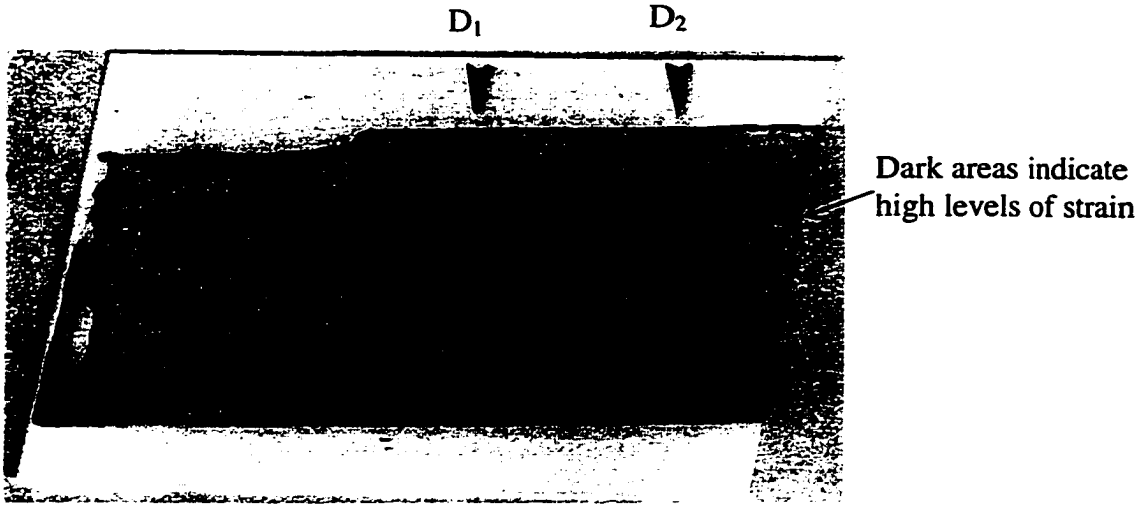

Figure 4.5 X-ray surface topograph in the [010] direction of the macro sodium nitrate crystal

Hillocks H_1 and H_2 correspond with the dislocation bundles D_1 and D_2. The dark lines on the topograph are indicative of high levels of strain and of dislocations. The dark layer, from which the dislocations propagate, is formed during the refacetting of the macro crystal when the crystal is again subjected to supersaturated solution conditions. The crystal has regions of high strain and dislocation bundles. At low supersaturations this supports the theory that the growth rate is dislocation controlled. The enhancement due to these bundles can effect the growth rate to an extent but it will not be a large effect due to the low level of growing supersaturation.

Conclusions

Integral strain analysis of sodium nitrate secondary nuclei demonstrates that crystal growth rates have a higher dependence upon strain at higher levels of growing supersaturation than they do at low levels. This correlates well with the results and predictions of Jones and Larson (1999a), where they predict that nuclei growth rates are strain

controlled at high growing supersaturations and dislocation controlled at low growing supersaturations.

The growth rates of sodium nitrate crystals at low levels of relative supersaturation, $\sigma<0.45\%$, are controlled by a dislocation mechanism. The close fit of the BCF model to the experimentally derived growth rates demonstrated that at the low levels of growing supersaturation the growth rate was dislocation controlled. At higher supersaturations it was not possible to identify the growth mechanism due to massive nucleation in the cell.

Surface topography of the crystal demonstrated that growth hillocks on the laser interferogram correspond with dislocation bundles in the X-ray surface topograph. These dislocation bundles serve as both growth sources and sources of strain, but at low levels of growing supersaturation it was the dislocations that were growth rate controlling. The dislocations propagated along with the growth of the crystal face.

References

Burton, W. K., N. Cabrera, and F. C. Frank, The Growth of Crystals and the Equilibrium Structure of their Surfaces, *Phil. Trans. Roy. Soc.* 243(1951), 299-358.

Jones C. M., and Larson, M. A., Characterizing Growth Rate Dispersion of $NaNO_3$ Secondary Nuclei as a Function of Supersaturation, paper submitted to *AIChE J.* January 1999.

Jones C. M., and Larson, M. A., Using Dislocations And Integral Strain To Model The Growth Rates Of Secondary Nuclei, paper submitted to *Chem. Eng. Sci.* March 1999.

Ristic, R.I., J. N. Sherwood, and T. S. Shripathi, The Role of Dislocations and Mechanical Deformation in Growth Rate Dispersion in Potash Alum Crystals, *Advances in Industrial Crystallization,* (Butterworth-Heinemann, Oxford, 1991) pp. 77-91.

Ristic, R.I., J. N. Sherwood, and T. S. Shripathi, The influence of tensile strain on the growth rates of potash alum and sodium nitrate, *J. Cryst. Growth,* 179(1997), 194-204.

Ristic, R. I., J. N. Sherwood, K. Wojciechowsky, Assessment of the Strain in Small Sodium Chlorate Crystals and its Relation to Growth Rate Dispersion, *J. Cryst. Growth*, 91(1988), 163-168.

CHAPTER 5. GENERAL CONCLUSIONS

General Discussion

Chapter 2

The initial growth rate distribution of sodium nitrate secondary nuclei is fit well by a gamma distribution. There is no detectable difference between the initial growth rate distributions of different faces of sodium nitrate and the growth rate distribution of the characteristic length. This follows because the faces of sodium nitrate are crystallographically equivalent.

The response of the mean, standard deviation, and the CV of the initial growth rate distribution are used to characterize growth rate dispersion for a system. Changing the supersaturation present during nucleation and during growth have varying effects on the initial growth rate distributions of sodium nitrate secondary nuclei. The mean and coefficient of variation of the initial growth rate distribution are dependent upon both the supersaturation at nucleation and the supersaturation during growth. The mean of the initial growth rate distribution increases with increasing nucleation supersaturation at low levels of growing supersaturation, and it decreases with increasing nucleation supersaturation at high levels of growing supersaturation.

Because strain is known to decrease crystal growth rates, and increasing dislocation density is known to increase crystal growth rates, it was proposed that crystal growth rates are dislocation controlled at low growing supersaturations and strain controlled at high levels of growing supersaturation. Only the growing supersaturation was shown to have a statistically significant effect on the standard deviation of the initial growth rate distribution.

Chapter 3

Single crystal growth rate experiments have shown that the growth rates of sodium nitrate secondary nuclei decrease over time following nucleation, while potash alum and potassium sulfate crystals nuclei growth rates remain constant over similar intervals of time. The time dependent behavior of the growth rates of sodium nitrate secondary nuclei is most likely due to the time dependence of sodium nitrate's growth rate to an initial level of strain. That is why the growth rates of sodium nitrate nuclei decrease as time passes. From the literature it is known that high dislocation densities correlate well with crystals having high growth rates.

Figures 3.8 and 3.9 show a high correlation between the initial growth rates of sodium nitrate secondary nuclei and the value of the growth rate deceleration. This leads one to conclude that a crystal has more chance of having strain not in equilibrium with the crystal lattice when it also has a high dislocation density. That also explains why secondary sodium nitrate nuclei with the highest growth rates will on average have the highest level of deceleration because they also have the higher levels of strain not in equilibrium within the lattice. One could call this higher levels of excess strain. It just takes time for it to incorporate itself into the lattice and effect the crystal growth rate. Slow growing sodium nitrate secondary nuclei probably have fewer growth sources. They may also have a large amount of integral strain that is already in equilibrium in the crystal lattice. It is the strain which has not yet come to equilibrium in the crystal that causes the decreasing growth rates.

Brittle substances such as potash alum and potassium sulfate do not exhibit time dependent growth rates following nucleation. In macro crystal experiments (Ristic *et al.*

1997), potash alum responded to applied strain with step changes in growth rate, while sodium nitrate responded with a linearly decreasing growth rate with respect to time. It was inferred from these results, that the ductility of the crystallizing material plays an important role in determining the growth rate profile of a crystal.

It was suspected that crystal growth rates were dependent upon dislocations and strain. The model proposed in Equation 3.3 allows for crystal growth rates to be dependent upon both. It is generally accepted that increasing nucleation supersaturation increases dislocation density and integral strain; the parameter ε used in Equation 3.3 is the enhancement due to bundling of dislocations thought to increase with increasing dislocation density. However, it is known from experiments that increasing dislocation density has the opposite effect of increasing integral strain on the growth rate of a crystal. The growth rate model in Equation 3.3 is based on the idea that crystals will have distributions of integral strain and ε thereby causing a distribution of growth rates. The exact dependence of the ε and integral strain distributions upon the nucleation and growing supersaturations are not known. The results of Jones and Larson (1999a) suggest regions of control for the two growth rate factors. From Jones and Larson (1999a) it is suspected that ε is growth rate controlling at low levels of growing supersaturation, while integral strain is growth rate controlling at high levels of growing supersaturation.

According to the model in Equation 3.3, increasing the growing supersaturation increases the range of possible growth rates for the growth rate distribution. This explains why the growing supersaturation showed up as a statistically significant factor effecting the

standard deviation of the growth rate distribution. The more possible values a growth rate can have the wider the distribution can be.

Chapter 4

Integral strain analysis of sodium nitrate secondary nuclei demonstrated that crystal growth rates are more dependent upon strain at higher levels of growing supersaturation than they are at low levels of growing supersaturation. This correlates well with the results and predictions of Jones and Larson (1999a). In that work it was proposed that nuclei growth rates are strain controlled at high growing supersaturations and dislocation controlled at low growing supersaturations. The data correlating nuclei growth rates with integral strain at different supersaturations validates that idea

The growth rates of sodium nitrate crystals at low levels of relative supersaturation, $\sigma<0.45\%$, are controlled by dislocations. Laser interferometry clearly displayed the growth hillocks on the crystal surface. At higher supersaturations it was not possible to identify the growth mechanism due to massive nucleation in the cell. And the good fit between the data points and the BCF model (Burton, *et al.* 1951) further demonstrated that claim was valid.

Surface topography of the crystal demonstrated that growth hillocks on the laser interferogram correspond with dislocation bundles in the X-ray surface topograph. Dislocation bundles are both sources for increasing growth and for strain. This is evident because the dislocations show up as dark regions on the surface topograph indicating high levels of strain. However, the growth rates of sodium nitrate crystals are not highly dependent upon the integral strain at low levels of supersaturation as demonstrated with the secondary nuclei.

Recommendations for Future Work

There is a need to investigate further into how the supersaturation present during nucleation effects the integral strain and dislocation density of secondary nuclei. Unfortunately, current techniques used to determine integral strain and dislocation density require a crystal to grow to an appreciable size.

Studying macro sized crystals has provided results that do not appear to contradict those seen with secondary nuclei. The refacetting process of a seed crystal may be thought of as an event similar to that of nucleation. This idea is now being tested in ongoing research by performing X-ray topography on secondary nuclei that have grown bigger than 600 microns. The idea is that if a strained core can be identified from which dislocations propagate then the two events are similar because a strained layer exists around the seed crystal after refacetting. The nucleation event would then be inferred to be the source of strain and dislocations, and the supersaturation conditions present during nucleation would have a direct effect upon both factors. Once the relationship between nucleation and refacetting seed crystals has been shown, experiments on macro crystals could be performed *en masse*. The results obtained for macro crystals could then be assumed to be true to a large extent for secondary nuclei as well.

Further work should be performed to ascertain the dependence of a crystallizing material's ductility upon it's growth rate. It is very interesting that the growth rate profiles of sodium nitrate differ so much from those of potash alum and potassium sulfate. Crystallizing materials of similar ductility to sodium nitrate would yield results that could either support or refute the ideas supported in this dissertation.

It would be beneficial to determine what the integral strain distribution and the distribution of ε, the growth rate enhancement due to bundling of dislocations, are for a population of crystals. Knowledge of these distributions, and how they might vary with respect to changing crystallizer conditions, would provide valuable insight into how the growth rate distribution can be influenced for a given crystallizer system. A mathematical dependence for the growth rate distribution would also be possible after determining the distributions of the integral strain and ε.

References

Jones C. M., and Larson, M. A., Characterizing Growth Rate Dispersion of $NaNO_3$ Secondary Nuclei as a Function of Supersaturation, paper submitted to *AIChE J.* January 1999.

Jones C. M., and Larson, M. A., Using Dislocations And Integral Strain To Model The Growth Rates Of Secondary Nuclei, paper submitted to *Chem. Eng. Sci.* March 1999.

Ristic, R.I., J. N. Sherwood, and T. S. Shripathi, The influence of tensile strain on the growth rates of potash alum and sodium nitrate, *J. Cryst. Growth,* 179(1997), 194-204.

ACKNOWLEDGMENTS

I would like to thank Dr. Wayne Genck of Genck International for his financial support the past three years. I would like to thank Dr. Jacobson for his support and information about X-ray diffraction techniques. I would like to thank Dr. Stephenson for his statistical advice. Much of what I did was dependent upon statistical analysis and Dr. Stephenson helped a lot with that. I would like to thank Dr. Ristic and Dr. Sherwood for their collaborative efforts and discussions about this work. They were very helpful with their critiques and their suggestions. I would like to thank Seth Holmen for his assistance. He did a wonderful job as an undergraduate assistant doing a lot of boring and repetitious crystal size measurements. I would like to thank Dr. Larson for being a great major professor. He is a model researcher, teacher, adviser, and friend, and I am thankful every day that I was able to have him for my major professor. He always gave me a lot of room to be creative and to try new ideas, while always being there to steer me in the right direction. I would like to thank my wife, Amy, for putting up with my wanting to go to graduate school and get my Ph.D. I know it was not always easy. I would also like to thank the graduate students and faculty in the department for always being friendly, helpful, and professional. You have all made my time here very positive and memorable. Thank you.

IMAGE EVALUATION
TEST TARGET (QA-3)

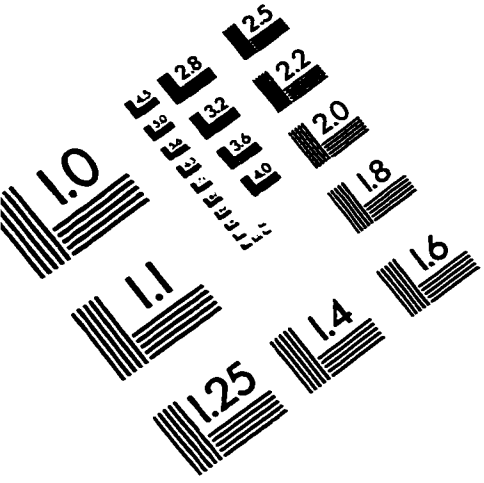

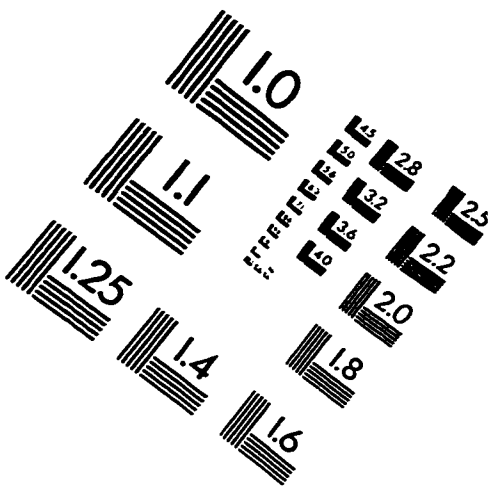

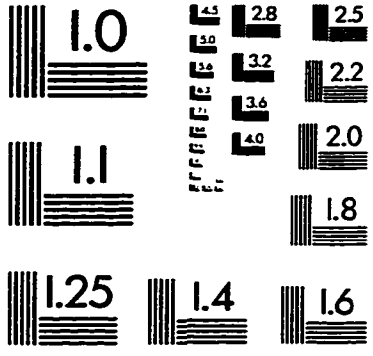

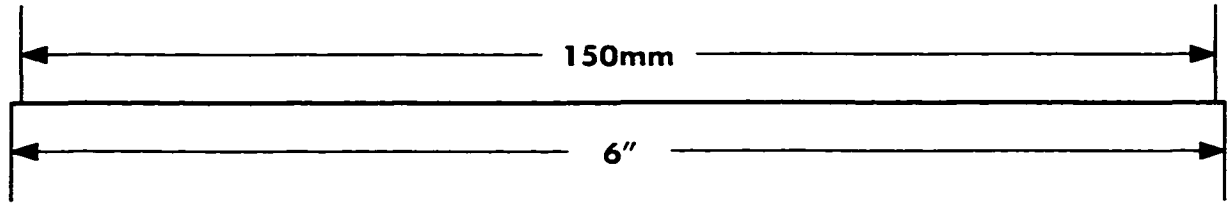

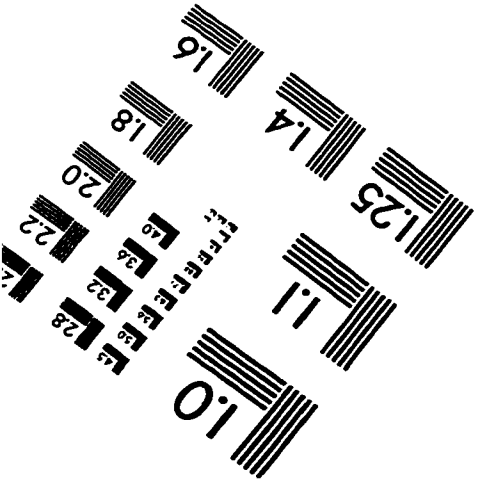

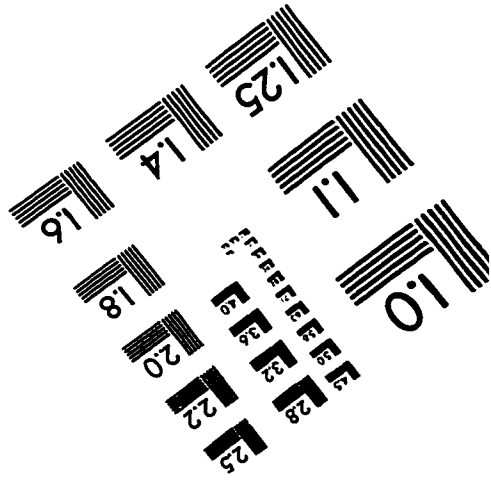

APPLIED IMAGE, Inc
1653 East Main Street
Rochester, NY 14609 USA
Phone: 716/482-0300
Fax: 716/288-5989

© 1993, Applied Image, Inc., All Rights Reserved